Lithos 348–349 (2019) 105181

Contents lists available at ScienceDirect

Lithos

journal homepage: www.elsevier.com/locate/lithos

Pyroxene-bearing low- and high-HREE TTGs from the northeastern margin of the Kaapvaal Craton, southern Africa: Implications for Archean geodynamics

H.M. Rajesh [a,*], G.A. Belyanin [b], O.G. Safonov [c,d,b], D.D. Van Reenen [b]

[a] Department of Earth and Environmental Sciences, BIUST, Botswana
[b] Department of Geology, University of Johannesburg, South Africa
[c] Korzhinskii Institute of Experimental Mineralogy RAS, Chernogolovka, Russia
[d] Department of Petrology, Geological Faculty, Moscow State University, Russia

ARTICLE INFO

Article history:
Received 10 July 2019
Received in revised form 20 August 2019
Accepted 22 August 2019
Available online 26 August 2019

Keywords:
Pyroxene-bearing TTG
Charnockite
Low-HREE TTG
High-HREE TTG
Southern Marginal Zone
Archean geodynamics

ABSTRACT

Archean tonalite-trondhjemite-granodiorite (TTG) rocks are generally amphibole- and/or biotite-bearing. Pyroxene-bearing granitoids of TTG affinity are less commonly reported. This study evaluates the range in composition and petrogenesis of pyroxene-bearing TTGs from a high-grade terrane along Archean cratonic margin. The Southern Marginal Zone high-grade terrane along the northeastern margin of the Kaapvaal Craton exposes prominent Mesoarchean pyroxene-bearing granitoids. The present study describes two groups of the granitoids in the Commissiedraai-Hugomond areas. The tonalite-trondhjemites with Fe-rich orthopyroxene (X_{Mg} = 0.46–0.49) dominate and occur as massive homogenous and banded varieties, the latter likely due to anatectic overprint. Enclaves of metabasites occur in both varieties. The darker layers of the banded variety are identical in mineralogy, texture and chemistry to the massive dark greenish-grey rocks. A less dominant group of clinopyroxene-rich massive tonalites occur in the Hugomond area. Clinopyroxene exhibit prominent orthopyroxene exsolution, with a pre-exsolution composition of X_{Mg} = 0.61–0.63. The spatially associated orthopyroxene-bearing and clinopyroxene-rich rocks are compositionally connected by a two-pyroxene-bearing variety with Mg-rich orthopyroxene (X_{Mg} = 0.56–0.59). No textures of pyroxene formation after earlier Fe—Mg minerals occur in the studied rocks, whereas textures of pyroxene destabilization are indicative of late magmatic interaction with a residual melt. Pyroxenes in all rocks are primary magmatic. Biotite-quartz intergrowths and amphibole after pyroxenes are late magmatic in origin. Small garnet crystals occur locally in the orthopyroxene-bearing tonalite-trondhjemites and are related to metamorphic/anatectic overprint. The rocks are affected by late alkali metasomatism close to shear zones. Geochemical characteristics of the orthopyroxene-bearing tonalite-trondhjemites are comparable to low-HREE TTGs, while that of the clinopyroxene-rich tonalites are similar to high-HREE TTGs. The proposed petrogenetic model considers the formation of both groups of pyroxene-bearing granitoids via remelting of mafic sources in a thickened plume-related oceanic plateau. The high temperatures of melting, low water activity and oxidized conditions likely resulted in the formation of charnockitic assemblages, and is supported by phase equilibria modelling. Shallow level melting of a MORB-like source produced clinopyroxene-rich high-HREE TTG. Subsequent melting of a slightly enriched-MORB-like source occurred at relatively greater depths forming orthopyroxene-bearing TTG with low-HREE characteristics. The two-pyroxene-bearing rocks likely resulted from the mingling-mixing of the high- and low-HREE TTG end members. Implications of the results on Archean geodynamics are discussed together with a comparative exercise with similar rocks from other Archean terranes.

1. Introduction

Granitoids occupying Archean crust include the Na-rich tonalite-trondhjemite-granodiorites (TTGs), K-rich granite-granodiorite-monzogranites (GGMs) and Mg-rich sanukitoids, the later characterizing the transition from Na-rich to K-rich granitoids (see recent reviews in Laurent et al., 2014a; Halla et al., 2017). These different granitoids are dominantly amphibole- and/or biotite-bearing. Pyroxene is not a common mineral of either TTGs (e.g., Moyen and Martin, 2012) or GGMs (e.g., Sylvester, 1994) except for the less silicic sanukitoids (e.g., Halla, 2005; Heilimo et al., 2010; Martin et al., 2010). The presence

* Corresponding author.
E-mail address: rajesh.hm@biust.ac.bw (H.M. Rajesh).

https://doi.org/10.1016/j.lithos.2019.105181
0024-4937/

of pyroxene instead of amphibole and/or biotite reflects the anhydrous nature of the granitoids and adds important constraints on the thermal state of the Archean felsic crust. An important aspect that needs clarification is whether this anhydrous nature is of primary or secondary origin? In other words, was pyroxene crystallized directly from the magma, or formed later as a result of high-temperature metamorphism and partial melting? Of the three groups of Archean granitoids, the question on the origin of pyroxene is most relevant for TTGs, as they formed throughout the Archean and constitute the dominant exposed Archean continental crust. A related question of significance is the origin of pyroxene-bearing TTGs. How far do the general arguments on the formation of Archean TTGs, which are polarized between two end-member settings – subducting oceanic lithosphere versus thickened oceanic plateau/oceanic crust (Bédard, 2006; Moyen and Martin, 2012; Smithies et al., 2009), applies to the formation of pyroxene-bearing TTGs is worth exploring. High-grade terranes along Archean cratonic margins are potential settings for pyroxene-bearing TTGs.

This paper describes pyroxene-bearing TTGs from the northeastern margin of the Archean Kaapvaal Craton in southern Africa. Field, petrographic, mineral chemical and bulk-rock geochemical characteristics of the Commissiedraai-Hugomond pyroxene-bearing granitoids are used to understand the mechanism of magma formation. Phase equilibria modelling is used to understand the formation conditions of the assemblages preserved in the rocks. As the northeastern margin of the Kaapvaal Craton constitute the southern part of the Limpopo Complex (Southern Marginal Zone), the results are compared with pyroxene-bearing granitoids from nearby (associated) high-grade terranes, including the southern margin of the Archean Zimbabwe Craton. The comparison is extended to similar rocks from other Archean terranes, thereby evaluating the significance of pyroxene-bearing TTGs in Archean geodynamics.

2. Geologic setting

2.1. Limpopo complex

The Paleoarchean to Paleoproterozoic Limpopo Complex is a high-grade (amphibolite- to granulite-facies metamorphic) terrane located between the Archean Kaapvaal and Zimbabwe cratons (Fig. 1a). It is subdivided into the Southern Marginal Zone along the northeastern margin of the Kaapvaal Craton, the Central Zone occupying the central and largest area of the Limpopo Complex, and the Northern Marginal Zone along the southern margin of the Zimbabwe Craton (Fig. 1b). The three zones are separated from one another and from the adjacent cratons by kilometre-scale shear zones (see reviews in Blenkinsop, 2011; Smit et al., 2011; Van Reenen et al., 2011). The Central Zone includes the Beit Bridge Complex, Phikwe Complex and the Mahalapye Complex terranes (Fig. 1b). Available estimates indicate that pyroxene-bearing granitoids constitute prominent rock units in the marginal zones (Berger et al., 1995; Bohlender et al., 1992; Du Toit,

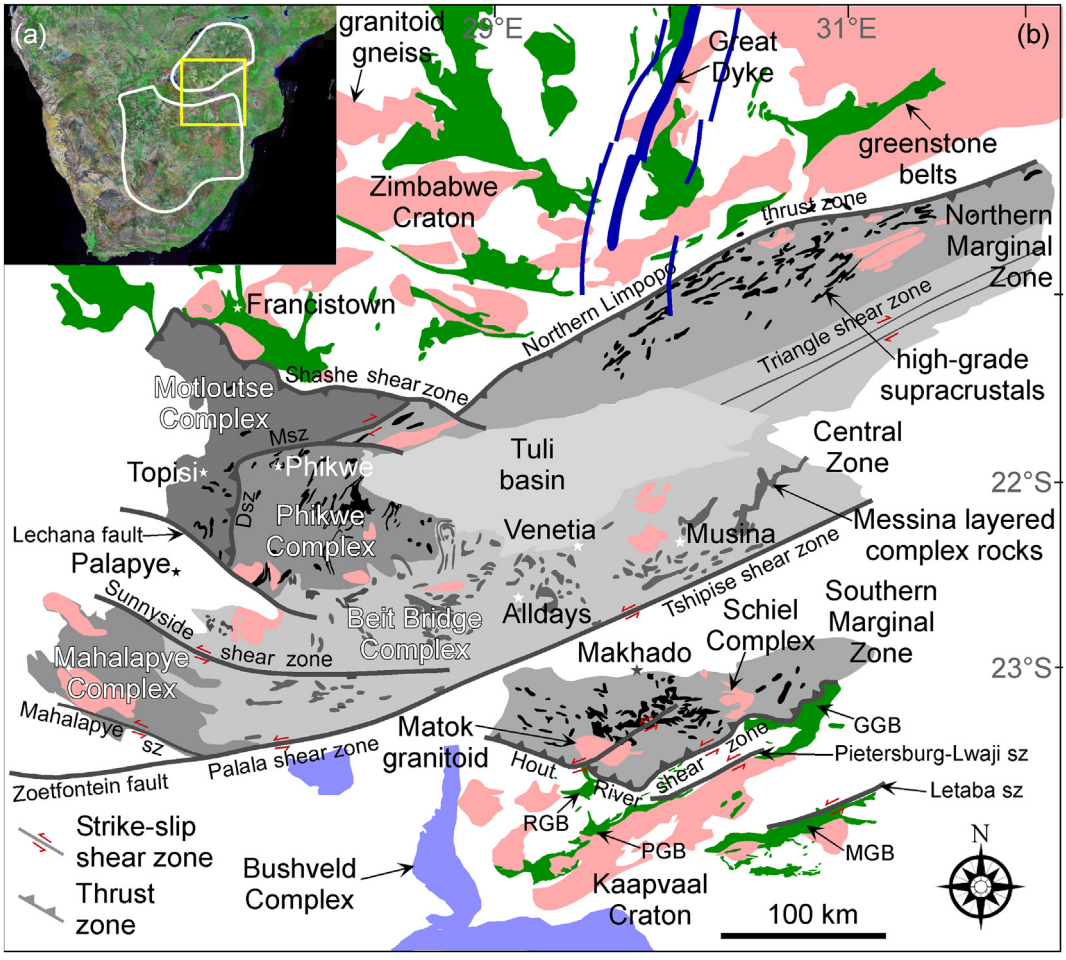

Fig. 1. (a) TM742 compilation of southern Africa showing the approximate extent of the Archean Kaapvaal and Zimbabwe cratons. The box indicates the area covered in (b). (b) Generalized geologic map of the Limpopo complex showing the approximate extents of the three zones, Southern Marginal Zone, Central Zone and Northern Marginal Zone, with respect to the adjacent cratons. Approximate extents of the different complexes – Beit Bridge Complex, Phikwe Complex and Mahalapye Complex, which form part the Central Zone, and Motloutse Complex – are also shown. Motloutse Complex to the southwest of the Zimbabwe Craton is not considered part of the Limpopo Complex. GGB – Giyani greenstone belt; RGB – Rhenosterkoppies greenstone belt; PGB – Pietersburg greenstone belt; MGB – Murchinson greenstone belt; sz – shear zone; Dsz – Dikalate shear zone; Msz – Magogaphate shear zone.

Please cite this article as: H.M. Rajesh, G.A. Belyanin, O.G. Safonov, et al., Pyroxene-bearing low- and high-HREE TTGs from the northeastern margin of the Kaapvaal Craton, southe..., Lithos, https://doi.org/10.1016/j.lithos.2019.105181

1994; Du Toit et al., 1983; Kreissig et al., 2000; Ridley, 1992). They are less prominent in the Central Zone (Laurent et al., 2011; Rajesh et al., 2018). The pyroxene-bearing TTGs studied here occur within the Southern Marginal Zone of the Limpopo Complex.

2.2. Southern marginal zone

The high-grade Southern Marginal Zone is juxtaposed against the low-grade (greenschist- to lower amphibolite-facies metamorphic) northeastern Kaapvaal Craton along the Hout River shear zone (Fig. 1b; Smit et al., 1992; Passeraub et al., 1999). It is bounded to the north by the Palala-Tshipise shear zone (Fig. 1b). The Southern Marginal Zone is dominantly composed of various tonalite-trondhjemite gneisses collectively referred to as the Baviaanskloof gneiss unit (Fig. 2). Available data on the different members of this unit indicate Mesoarchean crystallization ages. Ages of ~3.1 Ga (U—Pb zircon; no details given; Retief et al., 1990), 3121 ± 9 Ma, 3088 ± 11 Ma (U—Pb zircon; Rajesh et al., submitted) and 2981 ± 39 Ma (single $^{207}Pb/^{206}Pb$ zircon spot age; Vezinet et al., 2018) are known for pyroxene-bearing granitoids; ages of 3207 ± 5 Ma, 2922 ± 7 Ma, 2854 ± 8 Ma (U—Pb zircon; Vezinet et al., 2018) are reported for pyroxene-absent, biotite ± amphibole granitoids. The less dominant meta-mafic, meta-ultramafic and metasedimentary rocks of the Bandelierkop Formation form deformed discontinuous slivers within the voluminous Baviaanskloof gneiss unit (Fig. 2; Du Toit et al., 1983; Van Reenen et al., 2011). The metasedimentary rocks contain detrital zircons ranging from 3444 to 2733 Ma with prominent peaks at ca. 2940 and 2750 Ma (Nicoli et al., 2015; Rajesh et al., 2014; Taylor et al., 2014). An anthophyllite-in (Ath-in) isograd subdivides the Southern Marginal Zone into two domains (Fig. 2). The meta-supracrustal rocks exposed north of the Ath-in isograd are in the granulite-facies. Similar rocks within a narrow zone to the south of this isograd have been rehydrated under the amphibolite-facies (Van Reenen, 1986). The timing of granulite-facies metamorphism in the Southern Marginal Zone is constrained to ~2.72–2.71 Ga [2718 ± 7 Ma, 2716 ± 6 Ma, 2714 ± 22 Ma: Rajesh et al., 2014; 2713 ± 5 Ma, 2714 ± 6 Ma: Taylor et al., 2014; 2713 ± 8 Ma: Nicoli et al., 2015; 2705 ± 10 Ma, 2707 ± 13 Ma: Vezinet et al., 2018; all U—Pb zircon rim ages]. The Annaskraal, Petronella and Matok shear zones (Smit et al., 1992) separate the domain north of the Ath-in isograd into large crustal blocks (Fig. 2).

The kinematic indicators in the Southern Marginal Zone rocks indicate southwest thrusting of the high-grade rocks over the low-grade granite-greenstone terrane (Pietersburg block) of the Kaapvaal Craton along the Hout River shear zone between ~2.75 Ga and 2.62 Ga [2729 ± 19 Ma (Pb—Pb stepwise leaching method – titanite), 2712 ± 37 Ma (staurolite), 2691 ± 20 Ma (garnet), 2672 ± 51 Ma (kyanite); all ages from schists in the contact zone; Smit et al., 1992; Passeraub et al., 1999; Kreissig et al., 2001]. The early stage of exhumation of the Southern Marginal Zone is constrained by the U—Pb monazite age of 2691 ± 7 Ma on migmatitic metapelite (Kreissig et al., 2001). The period ~2.68–2.64 Ga is manifested by a number of late-tectonic intrusions into the Southern Marginal Zone. The largest is the ~2.68 Ga Matok pluton, a granitoid body occurring on either side of the Nthabalala shear zone (Fig. 2), and composed of 2686 ± 7 Ma to 2679 ± 7 Ma pyroxene-bearing granitoids and 2688 ± 8 Ma to 2679 ± 9 Ma pyroxene-absent, amphibole-biotite granitoids (all U—Pb zircon ages; Bohlender et al., 1992; Zeh et al., 2009; Laurent et al., 2014b). Minor intrusions are represented by garnet-bearing leucocratic [2663 ± 4 Ma (U—Pb monazite); 2643 ± 1 Ma (single zircon Pb/Pb evaporation); Kreissig et al., 2001], granodioritic-trondhjemitic [2667 ± 9 Ma (U—Pb zircon); Du Toit et al., 1983; Belyanin et al., 2014; Safonov et al., 2018] and pegmatitic bodies [2680 ± 6 Ma (U—Pb zircon); Nicoli et al., 2015]. Overprint ages of this period are reported from rocks of the Bandelierkop Formation [2667 ± 10 Ma, 2664 ± 23 Ma (U—Pb zircon rim); Rajesh et al., 2014; 2666 ± 4 Ma (U—Pb monazite in the leucosome patches); Safonov et al., 2018]. The timing of rehydration in the zone to the south of the Ath-in isograd is constrained to 2670–2620 Ma [Ar—Ar amphibole; Kreissig et al., 2001; Belyanin et al., 2014).

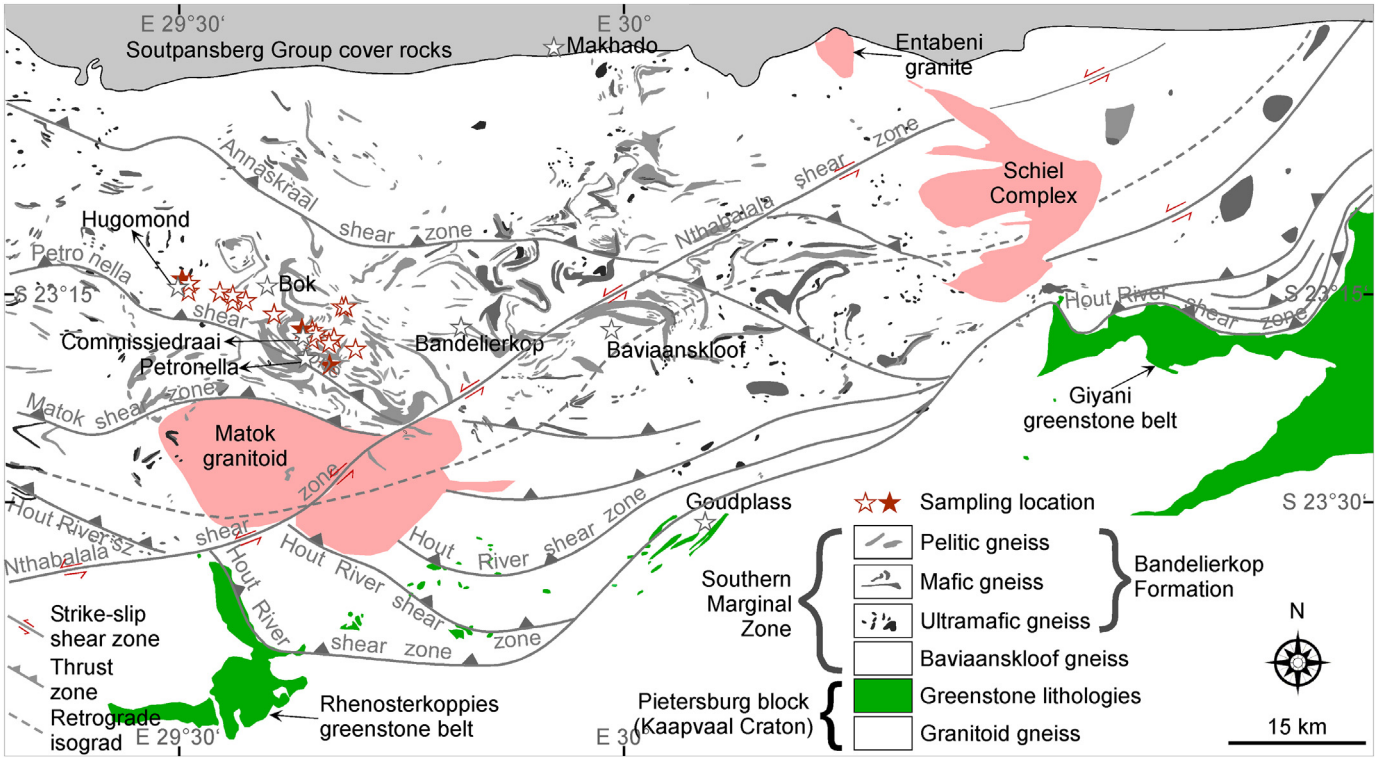

Fig. 2. Detailed geologic map of the Southern Marginal Zone showing the sampling locations (indicated by open red stars) (modified from Van Reenen et al., 2011). Three of these pyroxene-bearing granitoids were dated by Retief et al. (1990) and Rajesh et al. (submitted), and are shown by filled stars. The dated sample from the orthopyroxene-bearing banded granitoid is closer to the Petronella shear zone. (For interpretation of the references to colour in this figure legend, the reader is referred to the web version of this article.)

Post-tectonic Paleoproterozoic events within the Southern Marginal Zone involve the 2.06–2.05 Ga Schiel alkaline complex [2060 ± 4, 2050 ± 10 (Graupner et al., 2018)] and the ~2.02 Ga Entabeni granite [2023 ± 6 Ma (Zeh et al., 2009)] (Fig. 2), and overprint ages from different rock units [~2.06–1.9 Ga (Rb—Sr mica; Barton Jr. and Van Reenen, 1992); ~2.04–2.01 Ga (Ar—Ar amphibole-mica; Belyanin et al., 2014); ~1.9 Ga (U—Pb zircon rim; Rajesh et al., 2014)].

3. Field relations

Unlike the biotite±amphibole-bearing Na-rich TTG and K-rich granitoids from the terrane to the south of the Hout River shear zone, pyroxene-bearing granitoids are prominent in the Southern Marginal Zone. These granitoids, part of the Baviaanskloof gneiss unit (see Bohlender et al., 1992; Du Toit, 1994; Du Toit et al., 1983; Kreissig et al., 2000; Retief et al., 1990; Vezinet et al., 2018), are the less studied rocks of the Southern Marginal Zone.

The present study focuses on pyroxene-bearing granitoids occurring within and outside the extents of the Commissiedraai and Hugomond farms (Fig. 2). Similar granitoids are known from the Bok and Baviaanskloof farm areas (Fig. 2). A more deformed/metasomatised banded and migmatitic variety occurs in the Petronella and Baviaanskloof farm areas (Du Toit, 1994; Fig. 2). Together these pyroxene-bearing granitoids occur between the Petronella and Annaskraal shear zones (Fig. 2). Other occurrences of pyroxene-bearing granitoids (of the Baviaanskloof gneiss unit) are reported from south and north of the Petronella-Annaskraal corridor (Du Toit, 1994; Kreissig et al., 2000). Available data from previous studies are regarded for comparison.

Orthopyroxene-bearing and clinopyroxene-rich granitoids occur in the Commissiedraai-Hugomond areas. The orthopyroxene-bearing granitoids are prominently exposed in the Commissiedraai area. They occur as massive homogeneous light grey to darker greenish-grey variety (Fig. 3a, b) and banded variety with alternating greenish-grey and leucocratic layers (Fig. 3c, d). Often the leucocratic layers of millimetres to centimetres and sometimes even to meters in width have biotite-rich margins (Fig. 3d), indicative of at least partial in situ melting. Orthopyroxene is the main mafic mineral in both varieties. Garnet occurs locally in the granitoids. Mafic enclaves occur locally within the granitoids (Fig. 3b, c). These enclaves are darker and finer-grained relative to the granitoids and are locally folded (Fig. 3b, c). In contrast to the dominant orthopyroxene-bearing granitoids, a less dominant darker clinopyroxene-rich massive granitoid occur in the Hugomond area. Two pyroxene-bearing varieties occur along the contact zone between the orthopyroxene-bearing and the clinopyroxene-rich granitoids. These rocks exhibit textures indicative of mingling-mixing with darker rounded inclusions of clinopyroxene-rich rock in a lighter greenish-grey host. The contact between the two types of rocks is diffuse and gradual, with a layered appearance defined by thin dark clinopyroxene-rich layers in the light greenish-grey host. Pinkish alkali-metasomatic alteration zones occur in pyroxene-bearing granitoids closer to the Petronella and Nthabalala shear zones (Du Toit, 1994; Tsunogae and Van Reenen, 2014). The alteration is progressive with gradation from the unaltered grey/greenish-grey granitoid through less altered grey-pink rock to the most altered pink rock. Relict grey gneiss is preserved within the pinkish rock.

Retief et al. (1990) reported U—Pb zircon age of ~3.1 Ga from oscillatory zoned cores of prismatic grains with apparent $^{207}Pb/^{206}Pb$ ages of 2.9 to 3.1 Ga (no details provided) for clinopyroxene-rich granitoid from the Hugomond farm. They reported an overprint age of 2715 ± 5 Ma [quoted in Bohlender et al., 1992] in unzoned rim domains of zircon grains from the same rock. The Commissiedraai orthopyroxene-

Fig. 3. Field photographs illustrating the typical outcrop-scale appearance of massive (a, b) and banded (c, d) varieties of the Commissiedraai-Hugomond pyroxene-bearing granitoids. Inset in (b) is a close-up of darker fine-grained mafic enclave in the massive granitoid.

Please cite this article as: H.M. Rajesh, G.A. Belyanin, O.G. Safonov, et al., Pyroxene-bearing low- and high-HREE TTGs from the northeastern margin of the Kaapvaal Craton, southe..., Lithos, https://doi.org/10.1016/j.lithos.2019.105181

bearing granitoids show Mesoarchean crystallization ages [3088 ± 11 Ma (massive orthopyroxene-bearing), 3122 ± 9 Ma (banded orthopyroxene-bearing); see Fig. 2 for location of dated samples; Rajesh et al., submitted]. However, overprint ages notably differ, with 2706 + 50/−34 Ma from the massive orthopyroxene-bearing variety, and 1925 ± 19 Ma and 1976 ± 11 Ma from those in the orthopyroxene-bearing banded variety. The overprint age from the massive orthopyroxene-bearing granitoid is comparable to 2707 ± 13 Ma in unzoned rims of prismatic zircon grains from the 2981 ± 39 Ma (single $^{207}Pb/^{206}Pb$ zircon spot age from oscillatory zoned core) orthopyroxene-bearing granitoid from Baviaanskloof farm (Vezinet et al., 2018). The ~2.7 Ga ages are interpreted to represent metamorphic overprint ages, while the ~1.9 Ga age, obtained from granitoid occurring closer to the Petronella shear zone (see Fig. 2), is interpreted to represent age of local overprint on the orthopyroxene-bearing granitoids (Rajesh et al., submitted).

4. Petrography

Dominant medium-grained orthopyroxene-bearing granitoids are tonalite-trondhjemites containing up to ~55 modal % of plagioclase, up to ~35% of quartz, and up to ~10% of K-feldspar. The clinopyroxene-rich rocks are diorite-tonalites, while the two-pyroxene-bearing rocks are tonalites. Coarse subhedral plagioclase grains reflect a preserved magmatic texture (Fig. 4a–e). Triple junctions forming 120° angles, as part of polygonal granoblastic texture, do occur (Fig. 4c, d) but never widespread enough to infer significant high-temperature thermal annealing. Instead, irregular lobate grain margins, typical of magmatic crystallization, are prominent in the rocks (Fig. 4a, c–h). Weak biotite-defined foliation occurs locally. There is evidence for local deformation, especially in samples closer to the Petronella and Nthabalala shear zones, in the form of bent plagioclase grains, sutured quartzofeldspathic grain margins and recrystallized quartz grains.

Orthopyroxene content reaches up to ~10 modal% in the tonalite-trondhjemites (Fig. 4d, i). The dark layers of the banded variety are identical in mineralogy and texture to the massive dark greenish-grey rocks. The two-pyroxene-bearing tonalites (Fig. 4e, g, l–n) show increase in clinopyroxene content and decrease in orthopyroxene content relative to the orthopyroxene-bearing rocks. The darker diorite-tonalite contain up to 10 modal% clinopyroxene (Fig. 4h, j, k). Orthopyroxene exsolution lamellae are common in clinopyroxene grains (Fig. 4h, j). The lamellae are restricted to cores of the grains surrounded by thin exsolution-free rims (Fig. 4h). Both pyroxenes also form separate grains in the two pyroxene-bearing rocks. Amphibole locally replaces clinopyroxene (Fig. 4m). The occurrence of large individual grains of amphibole is accompanied by decrease in the modal content of clinopyroxene. Rare clinopyroxene inclusions occur in biotite and amphibole (Fig. 4n). Biotite occurs either along the margin of quartz and feldspar or pyroxene. When associated with pyroxene, biotite can form fingery intergrowths with quartz parallel to biotite cleavage planes (Fig. 4o, p). Small garnet crystals occur locally in the orthopyroxene-bearing granitoids. No reaction relations between garnet and orthopyroxene were observed in the studied samples. However, Tsunogae and Van Reenen (2014) reported texture of garnet growth after orthopyroxene from an altered granitoid from the Commissiedraai farm. Based on the occurrence of very fine-grained quartz inclusions in the garnet, Tsunogae and Van Reenen (2014) inferred the reaction orthopyroxene + plagioclase ± melt = garnet + quartz. No garnet is present in the clinopyroxene-bearing tonalites.

Myrmekite and antiperthite occurs locally (Fig. 4j, k). Apatite, magnetite and ilmenite are the common accessory minerals (Fig. 4i–p). Magnetite is associated with pyroxene, biotite and biotite+quartz intergrowths. Ilmenite typically occurs along the margin of magnetite. Magnetite-ilmenite composite grains are more common in the two-pyroxene-bearing tonalite, relative to the orthopyroxene- or clinopyroxene-bearing rocks. Zircon, monazite and allanite are less common. Minor sericite and chlorite are present in the studied samples. Sulphides occur in the clinopyroxene-bearing rocks.

5. Mineral chemistry

Analytical microprobe conditions (see Supplementary material DR1) and the mineral chemical data (Table DR2) are given as online Supplementary Material, whereas a summary of the salient mineral chemical characteristics is given in Table 1.

Orthopyroxene shows X_{Mg} = Mg/(Mg + Fe) = 0.46–0.49, 0.03–0.21 wt% TiO_2, 1.29–1.6 wt% MnO and 2–2.6 wt% Al_2O_3 (Table DR2a) corresponding to the ferrosilite field of the pyroxene quadrilateral (Fig. 5; Morimoto et al., 1988). In comparison, orthopyroxene in the two pyroxene-bearing tonalites has X_{Mg} = 0.56–0.59, 0.06–0.14 wt% TiO_2, 0.9–1.12 wt% MnO and 0.54–0.77 wt% Al_2O_3 (Table DR2a) corresponding to the enstatite field of the pyroxene quadrilateral (Fig. 5).

Clinopyroxene with composition of $Wo_{43.9–49.8}En_{38–40.2}Fs_{11.3–15.9}$, contains 0.08–0.34 wt% TiO_2, 0.38–0.57 wt% MnO, 1–2.16 wt% Al_2O_3 and shows X_{Mg} = 0.64–0.73 (Table DR2b). Nearly all clinopyroxene compositions plot within the diopside field of the pyroxene quadrilateral (Fig. 5). The overlap of core (X_{Mg} = 0.64–0.73) and rim (X_{Mg} = 0.68–0.72) compositions, especially at the high X_{Mg} side, indicate interference of Mg-rich orthopyroxene lamellae in the clinopyroxene composition. Reintegration of the pre-exsolution clinopyroxene composition using defocused beam analyses gives Fe-rich composition ($Wo_{44.3–47.1}En_{35–36.3}Fs_{17.5–19.7}$), with 0.16–0.22 wt% TiO_2, 0.48–0.55 wt % MnO, 1.4–1.48 wt% Al_2O_3 and X_{Mg} = 0.61–0.63 (Table DR2b; Fig. 5). The orthopyroxene exsolution lamellae in clinopyroxene are too thin to get reliable analyses.

Biotite in the orthopyroxene-bearing (clinopyroxene-absent) rocks show X_{Mg} = 0.48–0.55 and 0.37–0.54 apfu (atoms per formula unit) Ti, 2.66–2.97 apfu Al, 0.54–1.06 wt% F (Table DR2c). In comparison, biotite in the clinopyroxene-bearing tonalites is Mg-rich with X_{Mg} = 0.56–0.62, and exhibit narrower compositional variation [Ti = 0.45–0.58 apfu, Al = 2.51–2.77 apfu, F = 0.2–0.42 wt%] (Table DR2c). Amphibole replacing clinopyroxene shows X_{Mg} of 0.51–0.54, Si of 6.48–6.54 apfu, Ca_B of 1.84–1.86 apfu and $(Na + K)_A$ of 0.53–0.62. It contains 0.18–0.24 apfu Ti, 1.69–1.83 apfu Al and 0.54–0.68 wt% F (Table DR2d). Garnet occurring locally in Fe-rich orthopyroxene-bearing rocks shows composition $Prp_{14–18}Alm_{64–71}$ with minor grossular and spessartine components (Table DR2d). Composition of felsic minerals is less variable. Anorthite [An (=Ca/Ca + Na + K)] content of plagioclase is An_{21}-An_{27} (Table DR2d). K-feldspar composition is $Or_{91–97}$ (Table DR2d).

6. Bulk-rock chemistry

Major, trace and rare-earth element bulk-rock chemical compositions of the rocks from the Commissiedraai-Hugomond areas are given in Table 2. Analytical conditions are given as online Supplementary Material (see Supplementary material DR1). The samples KCH1 to 10 (Table 2) represent the dominant orthopyroxene-bearing tonalite-trondhjemites. Eight of them are the massive variety and two were collected from the dark layers of the banded variety. They show no visible evidence for metamorphic overprint. No garnet-bearing sample was selected for bulk-rock chemical study. A K-feldspar-rich sample KCH11 (Table 2) was included to characterize the effect of alkali-metasomatism. GAB60 series samples (Table 2) contain clinopyroxene. Samples GAB60a to d contain both pyroxenes and represent an approximate traverse with increasing clinopyroxene content and decreasing orthopyroxene content from the contact zone of orthopyroxene-bearing and clinopyroxene-rich granitoids. Samples GAB60e and f are clinopyroxene-rich tonalites. The dominant orthopyroxene-bearing tonalite-trondhjemites are referred to as Commissiedraai opx-bearing tonalite-trondhjemite, while the clinopyroxene-bearing rocks are

Please cite this article as: H.M. Rajesh, G.A. Belyanin, O.G. Safonov, et al., Pyroxene-bearing low- and high-HREE TTGs from the northeastern margin of the Kaapvaal Craton, southe..., Lithos, https://doi.org/10.1016/j.lithos.2019.105181

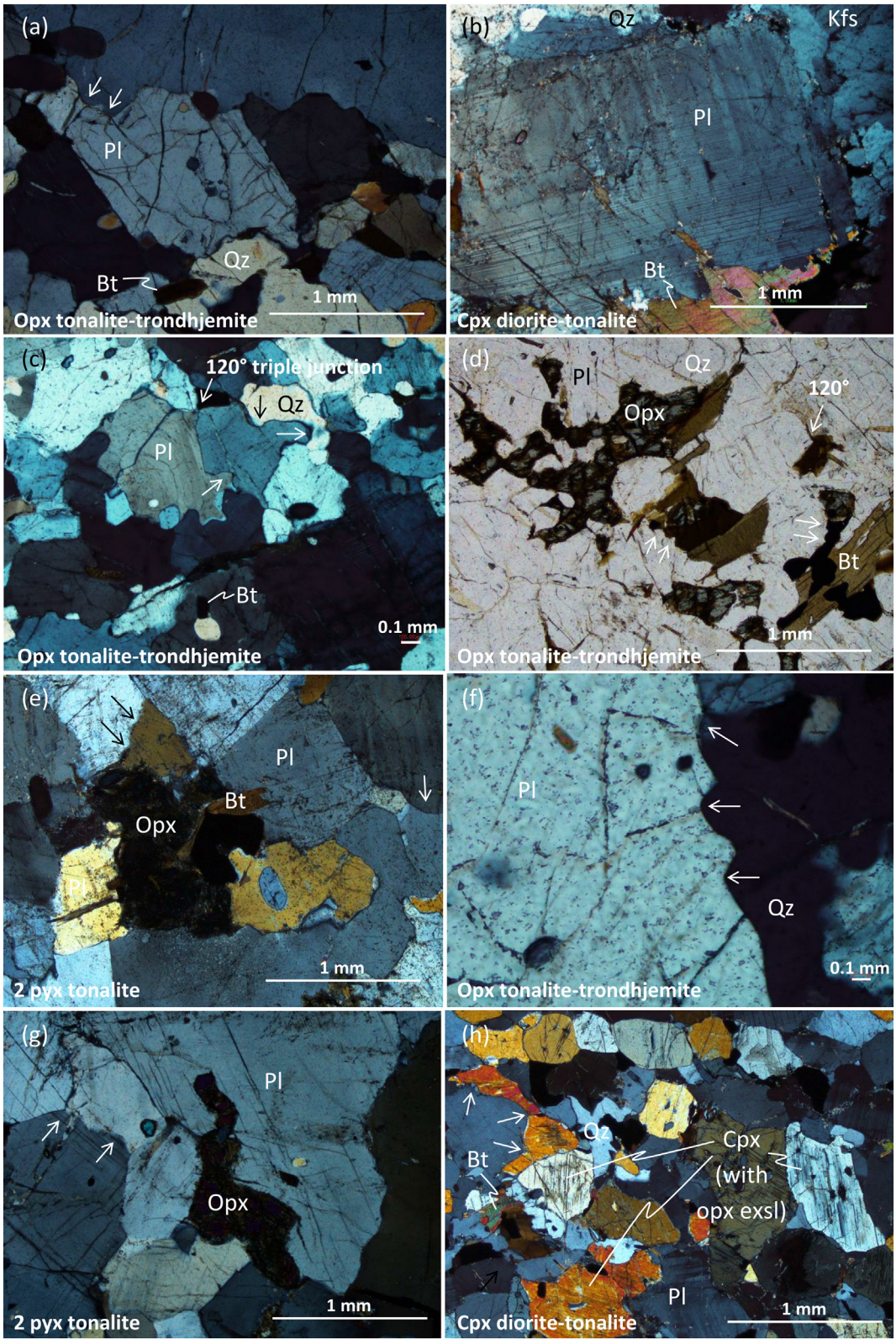

Fig. 4. Representative photomicrographs (a to h) and BSE images (i to p) illustrating the relation between the various rock forming minerals in the Commissiedraai-Hugomond pyroxene-bearing granitoids. The different features illustrated include the typical magmatic texture preserved in the studied samples (a to e), with occasional 120° triple junctions as part of polygonal granoblastic texture (c, d), prominent irregular lobate grain margins (indicated by arrows in a, c to h), mode of occurrence of orthopyroxene (d, e, g, i, l) and clinopyroxene with or without thin exsolution (exsl) lamellae of orthopyroxene (h, j, k), small grains of amphibole replacing clinopyroxene (m), rare clinopyroxene inclusion in biotite (n) and biotite+quartz replacing pyroxene (o, p). Except (d), all photomicrographs from (a to h) taken under crossed polarized light – (d) taken under plane polarized light. Pl – plagioclase; Qz – quartz; Kfs – K-feldspar; Opx – orthopyroxene; Cpx – clinopyroxene; Am – amphibole; Bt – biotite; Mt. – magnetite; Ap – apatite; Ilm – ilmenite; A – antiperthite.

Please cite this article as: H.M. Rajesh, G.A. Belyanin, O.G. Safonov, et al., Pyroxene-bearing low- and high-HREE TTGs from the northeastern margin of the Kaapvaal Craton, southe..., Lithos, https://doi.org/10.1016/j.lithos.2019.105181

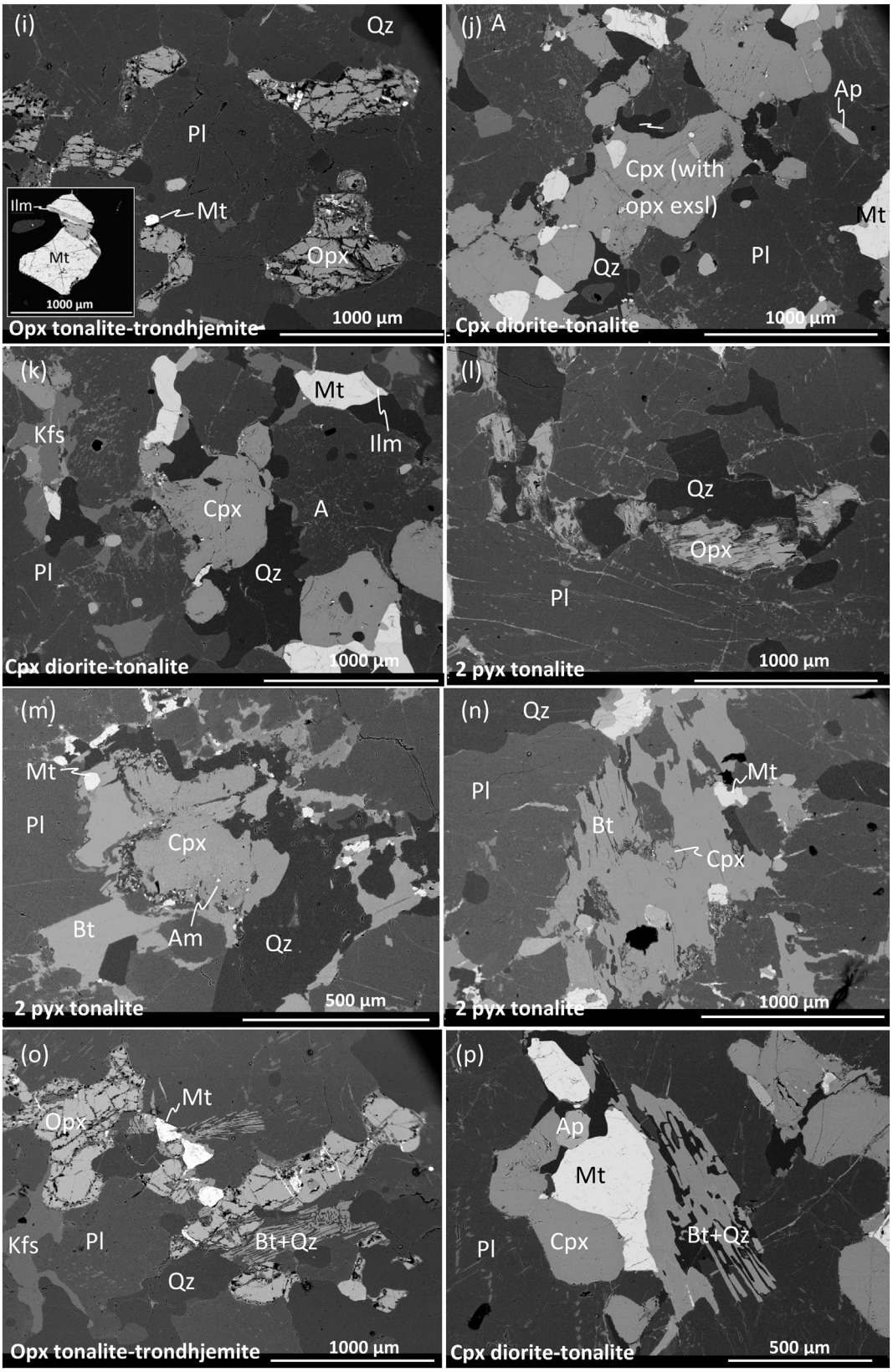

Fig. 4 (*continued*).

referred to as Hugomond two-pyx-bearing tonalite and Hugomond cpx-rich tonalite in the geochemical diagrams. Major and trace element data on close pairs of massive and banded (darker layers) varieties of orthopyroxene-bearing tonalite-trondhjemites from the Bok farm area [Van Reenen unpublished data (see Table DR3); Fig. 2] are included to understand the difference (if any) between the two varieties.

Massive and banded (darker layers) varieties of orthopyroxene-bearing tonalite-trondhjemites are similar in composition (see insets in Fig. 6). Except the alkali-metasomatised sample, all the pyroxene-bearing granitoids fall in the tonalite-trondhjemite fields of the normative An-Ab-Or triplot (Fig. 6a). The alkali-metasomatised sample corresponds to the granite field. This is comparable to the trend observed for alkali-metasomatised pyroxene-bearing granitoids sampled along a traverse by Tsunogae and Van Reenen (2014) from Commissiedraai farm (highlighted by arrowed line in inset of Fig. 6a). The orthopyroxene-bearing tonalite-trondhjemites are mildly peraluminous [ASI = molar Al/(Ca – 1.67P + Na + K) = 1.02–1.06] with SiO_2 contents of ~71–74 wt%. The two pyroxene-bearing tonalites containing ~63–68 wt% SiO_2 are metaluminous (ASI = 0.85–0.96). The clinopyroxene-rich tonalite has the lowest SiO_2 content (~58–59 w.%) and is metaluminous (ASI = 0.75–0.76) (Fig. 6b). All the pyroxene-bearing granitoids are magnesian in terms of Fe-number [FeO_t/(FeO_t + MgO)] (Fig. 6c) and calcic in terms of the modified alkali index (Na_2O + K_2O-CaO) (Fig. 6d).

The clinopyroxene-bearing tonalites have higher TiO_2, Al_2O_3, Fe_2O_3, MnO, MgO, CaO, Na_2O, P_2O_5, Co, Ga, Hf, Sr, V, Zr, Y and lower K_2O, Ba, Rb than the orthopyroxene-bearing tonalite-trondhjemites (Fig. 7; Table 2). The difference becomes quite apparent in terms of major and trace element ratios (Fig. 7; Table 2). The clinopyroxene-bearing tonalites show higher Mg# (~36–43), Ba/Rb (~30–50), Zr/Nb (~24–53), Zr/Hf (~36–41), La/Th (~34–92) and Gd/Yb (~2.6–3.4), and lower Sr/Y (~14–43), Nb/Y (0.36–0.53), Rb/Sr (0.01–0.02), Th/U (1.5–4), Th/Co (~0.01–0.05), La/Yb (~11–27) and K_2O/Na_2O (~0.18–0.20) than the orthopyroxene-bearing tonalite-trondhjemites (Mg# = ~32–41; Ba/Rb = ~5–8; Zr/Nb = ~9–26; Zr/Hf = ~31–36; La/Th = ~4–9; Gd/Yb = ~1.6–2.4; Sr/Y: ~31–54; Nb/Y = 0.46–1.02; Rb/Sr = ~0.11–0.18; Th/U = 8.5–50; Th/Co = ~0.4–1.5; La/Yb = ~22–31; K_2O/Na_2O = 0.29–0.46).

Primitive mantle-normalized (Sun and McDonough, 1989) multi-element spidergram for orthopyroxene-bearing tonalite-trondhjemites indicates enrichment in large ion lithophile element (LILE) and depletion in high field strength element (HFSE) (Fig. 8a). In comparison, the pattern of clinopyroxene-bearing tonalites are characterized by lower LILE and higher HFSE contents, with a progression from low to high contents observed among the two-pyroxene-bearing tonalites (Fig. 8a). In spite of the differences, both orthopyroxene-bearing and clinopyroxene-bearing granitoids show systematic negative Nb, Ta and Ti anomalies (Fig. 8a). A similar scenario is seen for the chondrite-normalized (Sun and McDonough, 1989) rare earth element (REE) patterns, with both orthopyroxene-bearing and clinopyroxene-bearing granitoids characterized by light REE (LREE) enrichment [$(La/Sm)_N$ = 6.31–8.32 (opx), 3.21–5 (two-pyx), 2.45–2.64 (cpx-rich)], heavy REE (HREE) depletion [$(Gd/Yb)_N$ = 1.33–2.01 (opx), 2.26–2.78 (two-pyx), 2.12–2.25 (cpx-rich)] and variable Eu anomalies [Eu/Eu* = 0.78–1.24 (opx), 0.87–1.35 (two-pyx), 0.62 (cpx-rich)] (Fig. 8b, Table 2). The REE patterns are slightly concave at the HREE end for the orthopyroxene-bearing tonalite-trondhjemites (Fig. 8b). The orthopyroxene-bearing tonalite-trondhjemites have $(La/Yb)_N$ = 15.95–23.49 with a regression from 10.62 to 19.16 in the two pyroxene-bearing tonalites to the lowest values of 7.75 to 8.18 in the clinopyroxene-rich tonalite (Table 2).

Table 1
Summary of salient mineral chemical characteristics of Commissiedraai-Hugomond pyroxene-bearing granitoids.

Mineral	Opx-bearing tonalite-trondhjemite	Two-pyx-bearing tonalite	Cpx-rich tonalite
Orthopyroxene	X_{Mg} = 0.46–0.49	X_{Mg} = 0.56–0.59	
Clinopyroxene		X_{Mg} = 0.69–0.73 (X_{Mg}^* = 0.62–0.63)	X_{Mg} = 0.64–0.71 (X_{Mg}^* = 0.61–0.63)
Biotite	X_{Mg} = 0.48–0.55	X_{Mg} = 0.56–0.60	X_{Mg} = 0.60–0.62
Amphibole		X_{Mg} = 0.51–54	
Garnet	X_{Mg} = 0.16–0.22		
Plagioclase	An_{21}-An_{27}	An_{25}-An_{27}	An_{25}-An_{27}

XMg = Mg/(Mg + Fe); XMg* – reintegrated pre-opx-exsolution composition; An = Ca/(Ca + Na + K)*100.

7. Discussion

To understand the significance of the Commissiedraai-Hugomond pyroxene-bearing granitoids, it is important to address their petrogenetic history. We start with first addressing the origin of pyroxenes in the studied granitoids. Phase equilibria modelling is used to understand the formation conditions of the observed assemblages in the pyroxene-bearing granitoids. Petrogenetic models are drawn in comparison to existing ones suggested for the origin of Archean TTGs. The

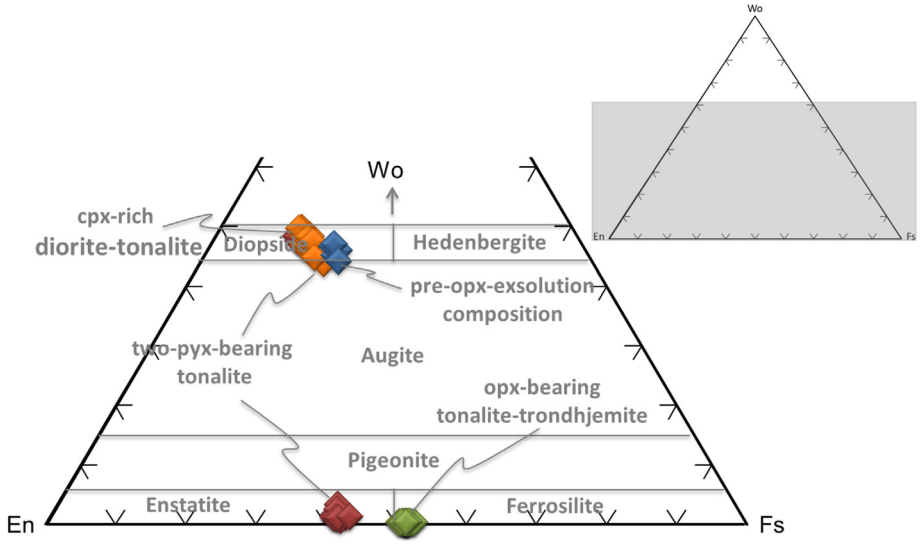

Fig. 5. Pyroxene compositions from the Commissiedraai-Hugomond granitoids [orthopyroxene(opx)-bearing tonalite-trondhjemite, two-pyroxene(pyx)-bearing tonalite, clinopyroxene (cpx)-rich diorite-tonalite) in the pyroxene quadrilateral. The pre-opx-exsolution composition of clinopyroxenes is also shown.

Please cite this article as: H.M. Rajesh, G.A. Belyanin, O.G. Safonov, et al., Pyroxene-bearing low- and high-HREE TTGs from the northeastern margin of the Kaapvaal Craton, southe..., Lithos, https://doi.org/10.1016/j.lithos.2019.105181

Table 2
Representative major, trace and rare earth element data for the Commissiedraai-Hugomond pyroxene-bearing granitoids.

	KCH1	KCH2	KCH3	KCH4	KCH5	KCH6	KCH7	KCH8	KCH9	KCH10	KCH11[a]	GAB60a	GAB60b	GAB60c	GAB60d	GAB60e	GAB60f
	Opx	Opx	Opx	Opx	Opx	Opx	Opx	Opx	Opx	Opx	Opx	Cpx + Opx	Cpx + Opx	Cpx + Opx	Cpx + Opx	Cpx	Cpx
SiO_2 (wt%)	73.60	72.98	73.22	72.34	73.24	73.67	72.97	73.61	72.64	72.48	74.45	68.02	67.14	66.98	63.23	58.94	59.38
TiO_2	0.17	0.17	0.14	0.20	0.17	0.14	0.16	0.17	0.18	0.19	0.12	0.30	0.51	0.47	0.53	0.82	0.81
Al_2O_3	14.41	14.44	14.61	14.83	14.29	14.12	14.43	14.29	14.68	14.72	13.39	15.46	15.62	15.90	16.57	16.17	15.96
Fe_2O_3[b]	2.01	2.35	2.15	2.47	2.22	2.30	2.41	2.11	2.02	2.51	2.08	3.93	4.03	3.93	5.00	7.39	7.27
MnO	0.02	0.04	0.03	0.05	0.04	0.03	0.04	0.03	0.03	0.05	0.02	0.05	0.06	0.06	0.07	0.11	0.11
MgO	0.56	0.65	0.55	0.84	0.70	0.52	0.60	0.60	0.67	0.79	0.50	1.10	1.32	1.32	1.71	2.69	2.68
CaO	2.61	2.59	2.55	2.90	2.66	2.51	2.56	2.71	2.57	2.82	1.79	4.07	4.45	4.48	5.64	6.92	6.85
Na_2O	4.40	4.39	4.48	4.69	4.51	4.40	4.45	4.57	4.36	4.60	3.45	4.80	4.89	4.93	5.14	4.87	4.98
K_2O	1.68	1.82	1.71	1.34	1.69	1.89	2.01	1.45	2.00	1.50	3.53	0.92	0.90	0.91	0.99	0.95	0.95
P_2O_5	0.05	0.04	0.04	0.04	0.05	0.04	0.05	0.05	0.08	0.05	0.07	0.14	0.17	0.18	0.19	0.26	0.24
Cr_2O_3	0.022	0.024	0.028	0.024	0.026	0.002	0.002	0.030	0.024	0.002	0.038	0.002	0.021	0.022	0.019	0.015	0.014
LOI	0.40	0.40	0.40	0.20	0.30	0.30	0.20	0.30	0.60	0.20	0.40	1.10	0.80	0.60	0.80	0.60	0.60
Total	99.93	99.89	99.91	99.92	99.90	99.92	99.88	99.92	99.85	99.91	99.84	99.89	99.91	99.78	99.89	99.74	99.84
ASI	1.05	1.04	1.06	1.03	1.02	1.02	1.02	1.02	1.05	1.03	1.06	0.96	0.92	0.93	0.85	0.76	0.75
MALI	3.47	3.62	3.64	3.13	3.54	3.78	3.90	3.31	3.79	3.28	5.19	1.65	1.34	1.36	0.49	−1.10	−0.92
Fe no.	0.78	0.78	0.80	0.75	0.76	0.82	0.80	0.78	0.75	0.76	0.81	0.78	0.75	0.75	0.75	0.73	0.73
Mg#	36.34	36.17	34.39	41.07	39.25	31.66	33.78	36.81	40.46	39.20	33.00	36.45	40.16	40.76	41.20	42.72	43.03
$Fe_TMgMnTi$	2.76	3.21	2.87	3.56	3.13	2.99	3.21	2.91	2.90	3.54	2.72	5.38	5.92	5.78	7.31	11.01	10.87
K_2O/Na_2O	0.38	0.41	0.38	0.29	0.37	0.43	0.45	0.32	0.46	0.33	1.02	0.19	0.18	0.18	0.19	0.20	0.19
Na_2O/K_2O	2.62	2.41	2.62	3.50	2.67	2.33	2.21	3.15	2.18	3.07	0.98	5.22	5.43	5.42	5.19	5.13	5.24
Q	35.29	34.07	34.45	32.58	33.94	34.80	33.15	34.92	33.34	32.90	36.49	26.91	24.87	24.30	17.07	11.72	11.81
C	0.73	0.63	0.85	0.49	0.32	0.37	0.40	0.39	0.86	0.52	0.81						
Or	9.93	10.76	10.11	7.92	9.99	11.17	11.88	8.57	11.82	8.86	20.86	5.44	5.32	5.38	5.85	5.61	5.61
An	12.62	12.59	12.39	14.13	12.87	12.19	12.37	13.12	12.23	13.66	8.42	17.92	18.01	18.57	19.22	19.45	18.39
Ab	37.23	37.15	37.91	39.69	38.16	37.23	37.65	38.67	36.89	38.92	29.19	40.62	41.38	41.72	43.49	41.21	42.14
Di												0.40	1.10	0.84	4.64	8.39	9.08
Hy	1.39	1.62	1.37	2.09	1.74	1.30	1.49	1.49	1.67	1.97	1.25	2.56	2.78	2.90	2.11	2.82	2.48
Ni (ppm)	<20	<20	<20	<20	<20	<20	<20	<20	<20	<20	<20	20	<20	15.8	21	23	21
Ba	270	320	279	188	266	323	351	205	365	201	827	186	205	206	186	208	191
Co	3.3	4.2	5.7	5.3	4.4	3.7	4	4.1	4.9	5	3.7	15.4	11.3	11.4	11.7	17.1	14.8
Cs	0.4	0.2	0.4	0.5	0.3	0.2	0.3	0.4	0.6	0.7	0.5	0.1	0.1	<0,1	0.1	0.1	0.1
Ga	12.1	13.2	13.7	13.8	12.9	12	12.5	12.8	12.9	13.3	11.2	14.1	14.7	15.5	16	19	17.9
Hf	1.8	2.3	2.1	2.4	2.3	2.2	2.5	2.5	1.9	2.3	2.6	4.5	4.2	4.4	6.1	6.4	6.3
Nb	4.8	3.8	4.1	6.1	3.2	3	3.3	4.3	7.2	5.7	4.2	3.3	5.7	5	6.5	10.2	9.7
Rb	38	39.8	40.7	33.2	38.3	40.4	45.5	34.7	53.7	38.6	81	5.8	4.1	5.2	6.2	6.8	6.2
Sr	272.5	280.2	281.3	293.6	269	287.1	275.4	272.9	296.9	279.4	299.9	359.1	393	384.6	391.4	404.8	391.6
Ta	0.4	0.2	0.2	0.4	0.2	0.2	0.2	0.3	0.5	0.6	0.5	0.3	0.2	0.3	0.8	0.8	0.8
Th	4.5	5.0	2.9	1.7	4	3.3	5.1	3.6	7.1	1.8	9.3	0.2	0.2	0.2	0.3	0.7	0.8
U	0.1	0.1	0.2	0.2	0.2	0.2	0.2	0.1	0.5	0.2	0.5	0.1	0.1	0.1	0.2	0.2	0.2
V	29	28.0	30	39	30	16	18	33	26	20	34	35	63	64	64	96	95
Zr	61.5	70.5	66.7	82.9	82.1	73.1	76.3	77.1	68	78.6	75.5	175.2	168.1	176.6	220.4	265.1	234.8
Y	7.3	6.7	5.2	6	7.1	6	7.2	6.1	9.7	6	10.4	8.3	10.8	11.5	17.9	25.4	27.2
La	23	22.6	18.7	14.9	21.2	19.6	24.3	21.7	25.9	15.9	27	17.9	17	18.4	23.1	29.2	27
Ce	43.3	42.6	33.9	26.9	41.5	35.7	45.1	40.2	52.5	28.1	52.3	34.5	34.2	38.5	49.2	67.2	64.3
Pr	4.47	4.6	3.52	2.74	4.04	3.52	4.56	3.97	5.24	2.77	5.67	3.76	4.18	4.69	5.96	8.61	8.37
Nd	15.4	15.9	11.7	9.4	13.1	11.2	15.6	14.1	18.5	9.6	18.3	14	16.4	18.1	24.6	35	35.3
Sm	1.92	2.2	1.7	1.4	2	1.52	2.16	1.85	2.65	1.37	3.07	2.31	3.03	3.52	4.64	7.15	7.11
Eu	0.55	0.6	0.56	0.52	0.57	0.58	0.56	0.55	0.61	0.52	0.62	1.02	1.05	1.13	1.29	1.46	1.4
Gd	1.8	1.5	1.1	1.08	1.56	1.27	1.53	1.35	2	1.2	2.4	2.25	2.74	3.07	4.27	6.97	6.4
Tb	0.22	0.2	0.14	0.15	0.22	0.17	0.2	0.19	0.27	0.17	0.29	0.28	0.37	0.43	0.62	0.98	0.91
Dy	1.28	1.1	0.9	0.98	1.17	0.94	1.23	0.97	1.54	0.95	1.66	1.61	2.19	2.28	3.41	5.71	5.38
Ho	0.23	0.2	0.18	0.17	0.2	0.2	0.21	0.18	0.32	0.2	0.32	0.27	0.38	0.41	0.66	1.06	0.99
Er	0.69	0.7	0.51	0.59	0.73	0.64	0.66	0.55	0.9	0.56	0.89	0.84	0.92	1.12	1.78	3.14	2.76
Tm	0.1	0.1	0.08	0.09	0.11	0.09	0.1	0.08	0.12	0.08	0.12	0.1	0.15	0.16	0.25	0.42	0.38
Yb	0.74	0.7	0.57	0.67	0.83	0.64	0.75	0.66	0.85	0.62	0.85	0.67	0.84	1.04	1.56	2.56	2.5
Lu	0.1	0.1	0.09	0.11	0.13	0.11	0.12	0.1	0.12	0.09	0.13	0.1	0.13	0.15	0.21	0.38	0.38
Ba/Rb	7.11	8.04	6.86	5.66	6.95	8.00	7.71	5.91	6.80	5.21	10.21	32.07	50.00	39.62	30.00	30.59	30.81
Rb/Sr	0.14	0.14	0.14	0.11	0.14	0.14	0.17	0.13	0.18	0.14	0.27	0.02	0.01	0.01	0.02	0.02	0.02
K/Rb	367.01	379.62	348.79	335.06	366.31	388.36	366.73	346.89	309.18	322.60	361.78	1316.79	1822.28	1452.76	1325.56	1159.77	1272.00
Sr/Y	37.33	41.82	54.10	48.93	37.89	47.85	38.25	44.74	30.61	46.57	28.84	43.27	36.39	33.44	21.87	15.94	14.40
Zr/Nb	12.81	18.55	16.27	13.59	25.66	24.37	23.12	17.93	9.44	13.79	17.98	53.09	29.49	35.32	33.91	25.99	24.21
Zr/Hf	34.17	30.65	31.76	34.54	35.70	33.23	30.52	30.84	35.79	34.17	29.04	38.93	40.02	40.14	36.13	41.42	37.27
Zr/Sm	32.03	31.47	39.24	59.21	41.05	48.09	35.32	41.68	25.66	57.37	24.59	75.84	55.48	50.17	47.50	37.08	33.02
La/Th	5.11	4.52	6.45	8.76	5.30	5.94	4.76	6.03	3.65	8.83	2.90	89.50	85.00	92.00	77.00	41.71	33.75
Nb/Y	0.66	0.57	0.79	1.02	0.45	0.50	0.46	0.70	0.74	0.95	0.40	0.40	0.53	0.43	0.36	0.40	0.36
Nb/Ta	12.00	19.00	20.50	15.25	16.00	15.00	16.50	14.33	14.40	9.50	8.40	11.00	28.50	16.67	8.13	12.75	12.13
Th/U	45.00	50.00	14.50	8.50	20.00	16.50	25.50	36.00	14.20	9.00	18.60	2.00	2.00	2.00	1.50	3.50	4.00
Th/Co	1.36	1.19	0.51	0.32	0.91	0.89	1.28	0.88	1.45	0.36	2.51	0.01	0.02	0.02	0.03	0.04	0.05
$(La/Sm)_N$	7.73	6.51	7.10	6.87	6.84	8.32	7.26	7.57	6.31	7.49	5.68	5.00	3.62	3.37	3.21	2.64	2.45
$(Gd/Yb)_N$	2.01	1.85	1.60	1.33	1.55	1.64	1.69	1.69	1.95	1.60	2.34	2.78	2.70	2.44	2.26	2.25	2.12

(continued on next page)

Please cite this article as: H.M. Rajesh, G.A. Belyanin, O.G. Safonov, et al., Pyroxene-bearing low- and high-HREE TTGs from the northeastern margin of the Kaapvaal Craton, southe..., Lithos, https://doi.org/10.1016/j.lithos.2019.105181

Table 2 (*continued*)

	KCH1	KCH2	KCH3	KCH4	KCH5	KCH6	KCH7	KCH8	KCH9	KCH10	KCH11[a]	GAB60a	GAB60b	GAB60c	GAB60d	GAB60e	GAB60f
	Opx	Opx	Opx	Opx	Opx	Opx	Opx	Opx	Opx	Opx	Opx	Cpx + Opx	Cpx + Opx	Cpx + Opx	Cpx + Opx	Cpx	Cpx
Eu/Eu[a]	0.89	0.89	1.17	1.24	0.95	1.24	0.90	1.02	0.78	1.21	0.67	1.35	1.09	1.03	0.87	0.62	0.62
$(La/Yb)_N$	22.29	23.49	23.53	15.95	18.32	21.97	23.24	23.58	21.86	18.40	22.78	19.16	14.52	12.69	10.62	8.18	7.75
$(Gd/Er)_N$	2.10	1.80	1.74	1.47	1.72	1.60	1.87	1.98	1.79	1.73	2.17	2.16	2.40	2.21	1.93	1.79	1.87

ASI – Aluminium saturation index; MALI – $Na_2O + K_2O$-CaO; Fe no. – total fe/(total Fe + MgO).
Mg# = 100.Mg/(Mg + Fe^{2+}); FeO = Fe_2O_3/1.15; $Fe_tMgMnTi$ = total Fe + MgO + MnO + TiO_2.
Q-C-Or-Ab-An-Di-Hy represent CIPW normative quartz, corundum, orthoclase, albite, anorthite, diopside, hypersthene values.
ASI = molar Al_2O_3/((CaO-1,67*P_2O_5) + Na_2O + K_2O); LOI – loss on ignition.
[a] Alkali-metasomatised.
[b] Total Fe as Fe_2O_3.

ensuing discussion, including a comparative exercise with similar rocks from other Archean terranes, evaluates the significance of the suggested model in Archean geodynamics.

7.1. The origin of pyroxenes in the Commissiedraai-Hugomond granitoids

An important question to address when dealing with pyroxene-bearing granitoids from high-grade terranes is whether the pyroxenes are of magmatic or metamorphic origin (e.g., Bédard, 2003; Percival, 1994; Rajesh et al., 2011). Du Toit (1994) pointed out the lack of relict igneous textures in the banded and migmatitic pyroxene-bearing granitoids from the Southern Marginal Zone. In contrast, magmatic textures are better preserved in the massive pyroxene-bearing granitoids (Du Toit, 1994; Fig. 4). In the Commissiedraai-Hugomond granitoids, orthopyroxene locally has an interstitial habit (Fig. 4) which is hard to explain otherwise than by crystallization from a magmatic mush. It also seems to be in textural equilibrium with biotite in places (Fig. 4) which is also at odds with metamorphic recrystallization, since these two phases are respectively reactant and product in many metamorphic reactions of the amphibolite-granulite transition. Orthopyroxene has low Al_2O_3 (<3 wt%) compared to those in high-T granulites (generally >5 wt%; see Harley, 2004). Reaction textures indicative of pyroxene formation after earlier Fe—Mg minerals are absent in the studied rocks. Therefore, we consider orthopyroxene and clinopyroxene as part of a primary magmatic assemblage in the studied granitoids (Fig. 4). The occurrence of biotite along grain margins as well as biotite-quartz intergrowths after pyroxenes (Fig. 4) argues for late magmatic formation of biotite close to solidus via reaction of pyroxene with potassic melt. A similar origin can be inferred for amphibole in the clinopyroxene-bearing granitoids. Very similar textures were observed and interpreted the same way in other ortho- and clinopyroxene-bearing granitoids (e.g., Frost et al., 2000; Ridley, 1992), including the nearby rocks from the Matok pluton (Laurent et al., 2014b).

7.2. Phase equilibria modelling of the pyroxene-bearing granitoids

Phase equilibria were modelled via Gibbs free energy minimization in the system MnO–Na_2O–CaO–K_2O–FeO–MgO–Al_2O_3–SiO_2–H_2O–TiO_2–O_2 (MnNCKFMASHTO) using the PERPLE_X software (Connolly, 2005) in version 6.7.7 for Windows. The standard properties database hp11ver.dat (Holland and Powell, 2011) and solution model database solution_model.dat (http://www.perplex.ethz.ch) were applied for modelling. The following models recommended by White et al. (2014) were applied for mineral solutions: "Bi(W)" for Ti and Fe^{3+}-bearing biotite, "Opx(W)" for Fe^{3+}-bearing orthopyroxene. The model "Cpx(HP)" was used for Fe^{3+}-bearing clinopyroxene (Holland and Powell, 1996). Models "Ilm(WPH)" for the Mg-Mn-Fe^{3+}-bearing ilmenite (White et al., 2000) and "MtUl(A)" for the magnetite-ulvospinel (Andersen and Lindsley, 1988) solid solutions were used to reproduce relations of ilmenite and magnetite in the rock. The model "feldspar", based on the solution model of Fuhrman and Lindsley (1988), was taken for ternary feldspar. The model "melt(W)" from White et al. (2014) was used for the NCKFMASH silicate melt.

7.2.1. Orthopyroxene-bearing tonalite-trondhjemite (KCH5)

Fig. 9a demonstrates a P-T pseudosection for the representative bulk composition of the orthopyroxene-bearing granitoid KCH5 (wt%): SiO_2–73.24, TiO_2–0.17, Al_2O_3–14.29, FeO – 1.998, MnO – 0.040, MgO – 0.70, CaO – 2.66, Na_2O – 4.51, K_2O – 1.69. A "free" O_2 (as a monitor of Fe_2O_3) content of 0.05 wt% was taken on the basis of the T-M_{O2} (M_{O2} – amount of O_2) pseudosection. This is an optimal O_2 content, which gives better convergence of mineral compositions and assures formation of magnetite in the system along with the Fe^{3+}-bearing biotite and orthopyroxene. The water content 0.23 wt% was taken as a maximum content, which can be accommodated in the subsolidus assemblage. This value is close to the bulk-rock loss on ignition (LOI) value 0.30 wt%.

The P-T pseudosection demonstrates that the sequence of mineral crystallization is practically independent of pressure (phase field boundaries are sub-vertical). The assemblage Opx + Pl + Mt. + Ilm + Qz, which can be considered as primary in the orthopyroxene-bearing granitoid, is stable with melt above ~860 °C. At these temperatures orthopyroxene shows X_{Mg} = 0.48–0.49 (see short-dashed isopleths) and about 2.5–2.6 wt% Al_2O_3 (isopleths are not shown) (Fig. 9a). These compositional characteristics are similar to those in the rock (Table DR2a). However, orthopyroxene is stable with the granitic (69–70 wt% SiO_2) melt only up to temperatures above 800–820 °C (depending on pressure), at which it reacts out to form biotite with X_{Mg} = 0.48–0.55 (long-dashed isopleths) consistent with the Mg-number of biotite in the rock (Table DR2c). The content of the melt at these conditions is just 0.3–0.4 vol%. It contains about 6 wt% H_2O and is potassic (K_2O/Na_2O ~1.5). This relation is reflected in presence of biotite+quartz textures after orthopyroxene in the rock (Fig. 4o). Biotite is the only Fe—Mg aluminosilicate at lower temperatures. The An content in plagioclase is varying within 21–23 mol% consistent with the composition of plagioclase in the rock (Table DR2d). Ilmenite is predicted to disappear with biotite-forming reactions at temperatures 800–820 °C, but Ti-bearing magnetite is still present. This observation reflects a primary-looking magnetite and secondary-looking ilmenite in the rock. The diagram shows formation of late ilmenite (below ~750 °C) along with magnetite probably because of exsolution from the Ti-bearing magnetite (see inset in Fig. 4i). The subsolidus assemblage is Bt + Pl + Kfs + Mt. + Ilm + Qz.

7.2.2. Clinopyroxene-rich tonalite (GAB60f)

Fig. 9b demonstrates a P-T pseudosection for the representative bulk composition of the clinopyroxene-bearing granitoid GAB60f (wt%): SiO_2–59.38, TiO_2–0.81, Al_2O_3–15.96, FeO – 6.542, MnO – 0.11, MgO – 2.68, CaO – 6.85, Na_2O – 4.98, K_2O – 0.95. A "free" O_2 (as a monitor of Fe_2O_3) content of 0.4 wt% was taken on the basis of the T-M_{O2} (M_{O2} – amount of O_2) pseudosection. This optimal O_2 content gives better convergence of mineral compositions as well as assures a formation of

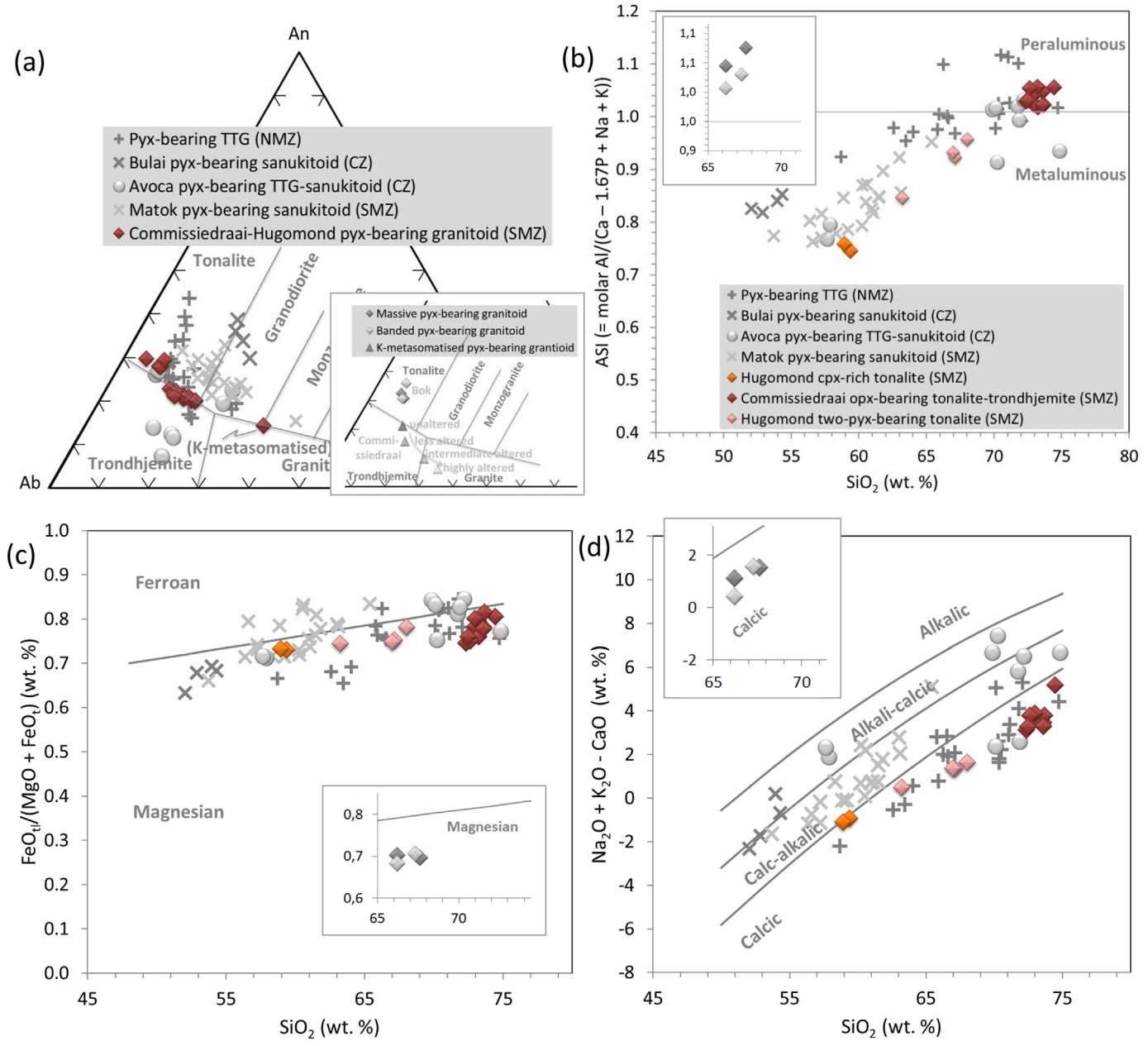

Fig. 6. Commissiedraai-Hugomond pyroxene-bearing granitoid compositions in terms of normative An-Ab-Or classification diagram of Barker (1979) (a), aluminium saturation index (ASI) vs SiO_2 plot (b), $FeO_t/(MgO + FeO_t)$ vs SiO_2 plot (c), and $Na_2O + K_2O$-CaO vs SiO_2 plot (d). All the studied pyroxene-bearing granitoids are grouped as one unit in (a). The legend in (b) applies to (c) and (d). Commissiedraai opx-bearing tonalite-trondhjemite constitute the dominant rock unit in the study area. Hugomond cpx-rich tonalite constitute the less dominant unit exposed near Hugomond farm. Hugomond two pyx-bearing tonalite represent the rock from the contact zone of the opx-bearing and cpx-rich end members. The insets in each diagram illustrate the comparison of close pairs of massive and banded (darker layers) varieties of orthopyroxene-bearing tonalite-trondhjemites from Bok farm area [Van Reenen unpublished data; see Table DR3]. Inset in (a) also shows the change in composition of alkali-metasomatised pyroxene-bearing granitoids from a traverse from unaltered to the most altered rock from the Commissiedraai farm area [compiled from Tsunogae and Van Reenen, 2014]. Available data on pyroxene-bearing granitoids of the Matok sanukitoid [from Laurent et al., 2014b] from the Southern Marginal Zone (SMZ), the Avoca TTG-sanukitoid (from Rajesh et al., 2018) and Bulai sanukitoid (from Laurent et al., 2011) from the Central Zone (CZ), and TTG (from Berger et al., 1995) from the Northern Marginal Zone (NMZ) are shown in the different diagrams. The fields in (c) and (d) are from Frost et al. (2001).

magnetite and Fe^{3+}-bearing ilmenite in the system along with the aegirine-rich jadeite-free high-Mg clinopyroxene. The water content 0.27 wt% was taken as a maximum content, which is accommodated in the subsolidus assemblage. This value is lower than the LOI value 0.60 wt%.

The simple P-T pseudosection demonstrates sub-vertical phase fields suggesting that the sequence of mineral crystallization is almost independent of pressure. The assemblage Cpx + Pl + Mt. + Ilm + Qz, which can be considered as primary in the clinopyroxene-rich granitoid, is stable with melt above ~870 °C. At these temperatures clinopyroxene shows X_{Mg} = 0.60–0.65 (short-dashed isopleths) depending on pressure. This Mg number of clinopyroxene is similar to that in the rock (Table DR2b). This assemblage includes small amount of orthopyroxene (below 0.5 vol%), which disappears with cooling. This feature could reflect a presence of abundant orthopyroxene lamellae in clinopyroxene grains (Fig. 4). The lamellae terminate at narrow lamellae-free clinopyroxene outer zones, suggesting that orthopyroxene is consumed by some reaction. In fact, disappearance of orthopyroxene is accompanied by formation of biotite, which show a clear late-magmatic origin in the rock. Biotite forms via reactions with a relatively sodic (K_2O/Na_2O ~ 0.5) melt and coexists with Cpx + Mt. + Ilm + Pl + Qz down to the subsolidus conditions.

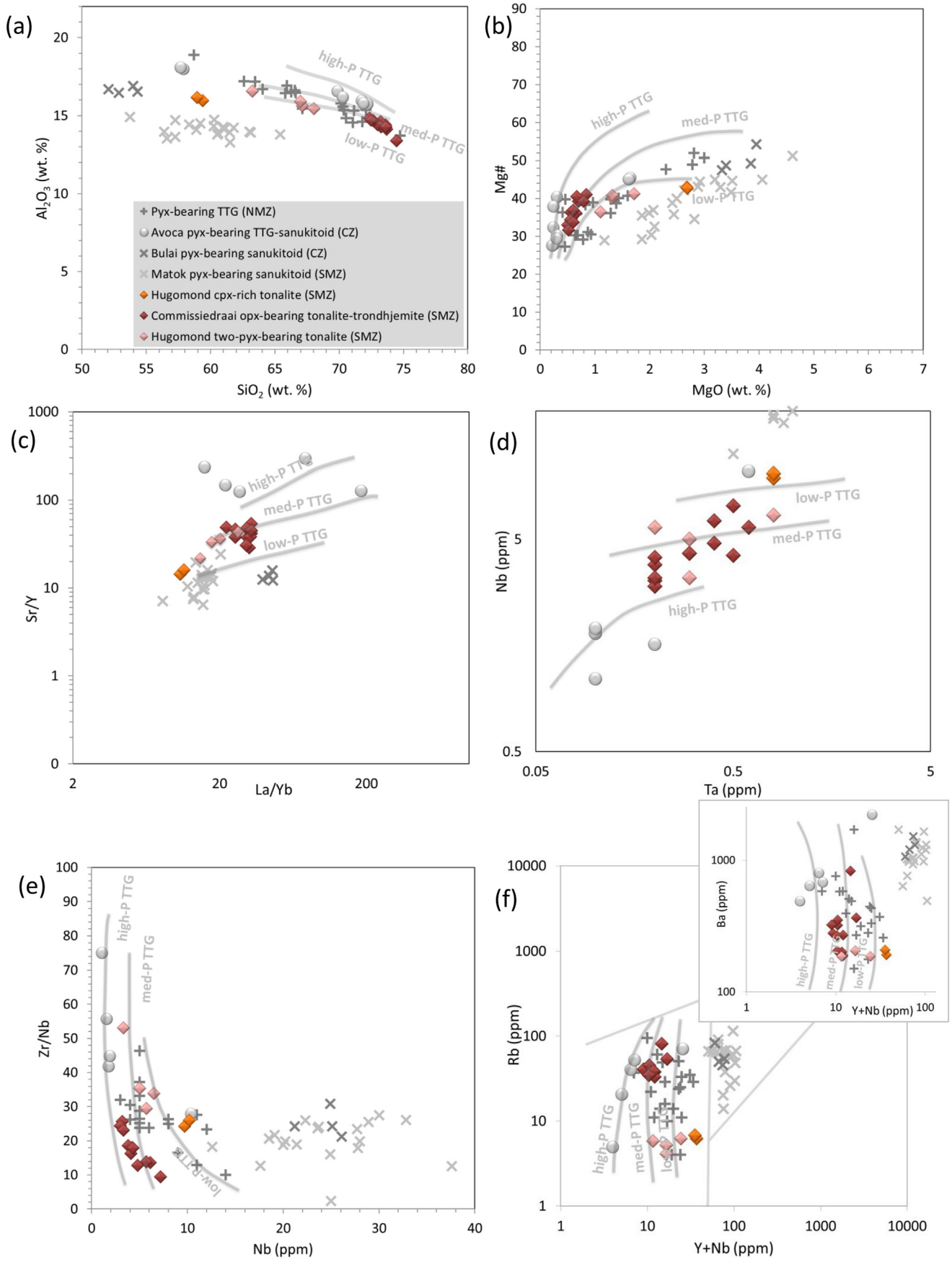

Fig. 7. Commissiedraai-Hugomond pyroxene-bearing granitoid compositions in terms of Al_2O_3 vs SiO_2 plot (a), Mg# vs MgO plot (b), Sr/Y vs La/Yb plot (c), Nb vs Ta plot (d), Zr/Nb vs Nb plot (e), and Rb vs Y + Nb plot (Ba vs Y + Nb plot – inset) (f). Approximate trends of high-pressure, medium-pressure and low-pressure TTGs are drawn based on respective fields as well as compilations from Moyen (2011). Fields in (f) are from Pearce et al. (1984). See caption of Fig. 6 for other details.

Please cite this article as: H.M. Rajesh, G.A. Belyanin, O.G. Safonov, et al., Pyroxene-bearing low- and high-HREE TTGs from the northeastern margin of the Kaapvaal Craton, southe..., Lithos, https://doi.org/10.1016/j.lithos.2019.105181

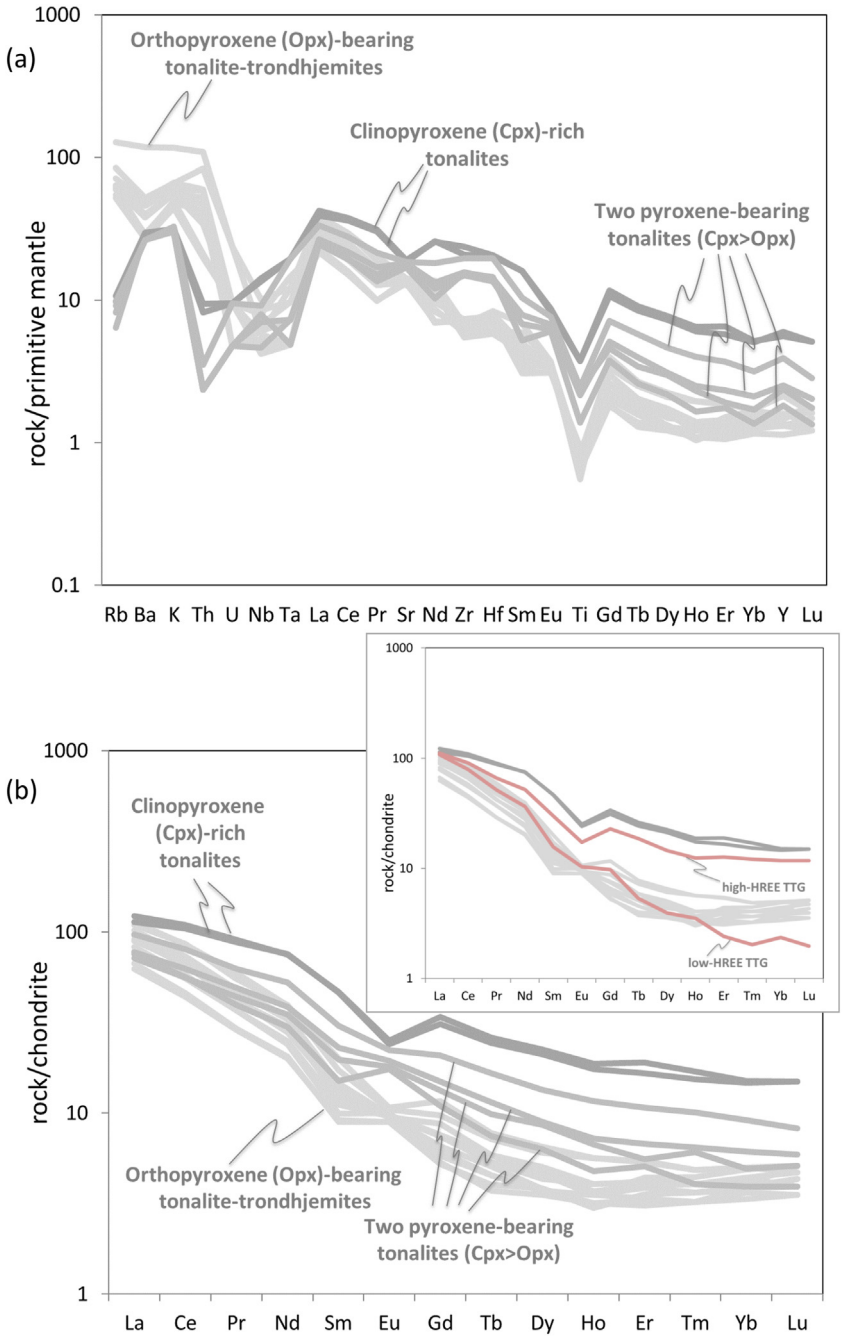

Fig. 8. Commissiedraai-Hugomond pyroxene-bearing granitoid compositions in terms of primitive mantle-normalized multi-element (a) and chondrite-normalized (Sun and McDonough, 1989) REE (b) plots. Inset in (b) compares the chondrite-normalized REE pattern of the pyroxene-bearing granitoids with that of typical low- and high-HREE TTGs from Halla et al. (2009).

7.3. Possible effect of overprint event(s) on the chemistry of the rocks

It is important to estimate the effect of overprint event(s) on the chemistry of the rocks. Geochronological data indicate two overprint events in the Baviaanskloof granitoids: ~2.72–2.71 Ga and ~2.06–1.91 Ga (Barton Jr. and Van Reenen, 1992; Vezinet et al., 2018; Rajesh et al., submitted). The *syn*-tectonic (~2.72–2.71 Ga) overprint event is reported from pyroxene-bearing granitoids near Hugomond and Baviaanskloof farm areas, and the post-tectonic (2.06–1.91 Ga) event reported from granitoids closer to the Petronella-Nthabalala shear zones (Fig. 2; Rajesh et al., submitted).

There is no prominent mineralogical evidence for metamorphic overprint in these granitoids. Only some textural features can be taken as the evidence for the metamorphic overprint. They are the 120° triple junctions forming polygonal granoblastic texture (e.g., Fig. 4c, d). The local appearance of garnet in the granitoids is debatable. The rare texture of garnet+quartz around orthopyroxene described by Tsunogae and Van Reenen (2014) could be related to metamorphic or anatectic overprint. As garnet is a minor phase and no particular structure or texture distinguish garnet-bearing rocks from garnet-free ones, the occasional presence of garnet can reasonably be considered as a second-order feature. This could be related to the Neoarchean event. Nevertheless, no garnet-bearing samples were selected for our geochemical study. The Paleoproterozoic ages likely correlate with the metasomatic overprint, and is supported by the ~2.04–2.01 Ga (Ar—Ar amphibole-mica; Belyanin et al., 2014) ages obtained on alkali-metasomatised rocks from the region. However, except one alkali-metasomatised sample, alteration is minimal in other studied samples.

Please cite this article as: H.M. Rajesh, G.A. Belyanin, O.G. Safonov, et al., Pyroxene-bearing low- and high-HREE TTGs from the northeastern margin of the Kaapvaal Craton, southe..., Lithos, https://doi.org/10.1016/j.lithos.2019.105181

The metamorphic overprint is also not evident from the geochemical characteristics of the rocks. Depletion in Rb, as indicated by high K/Rb ratios, is a common, but not an invariable feature of granulite-facies rocks (e.g., Rajesh et al., 2011; Rollinson, 1996). The bulk-rock K/Rb ratios of the orthopyroxene-bearing granitoids (~309–389) are similar to those found in common igneous rocks (~300–500; Table 2). The consistent and coherent trends in the different geochemical diagrams (Figs. 6, 7 and 8) argue for a lack of the overprint effect on the chemistry of the studied pyroxene-bearing granitoids. Thus, despite the geochronologic evidence, neither mineralogical nor geochemical effect of metamorphic overprint is seen in the studied rocks. Only 120° triple junctions are textural evidence of partial re-crystallization. Therefore, the samples can be used for petrogenetic reconstructions of the granitoid magma genesis.

7.4. Petrogenetic characterization of the pyroxene-bearing granitoids

Petrogenetic model for the granitoids needs to account for the spatial association of orthopyroxene-bearing and clinopyroxene-bearing rocks. They have contrasting mineral chemical characteristics (Table 1). Bulk-rock chemical characteristics of the rock types indicate similar trends, but are characterized by difference in concentration of elements. The clinopyroxene-bearing granitoids are more Mg-rich than the orthopyroxene-bearing ones (Figs. 6 and 7). These differences reflect either different sources or derivation from the same source under different conditions.

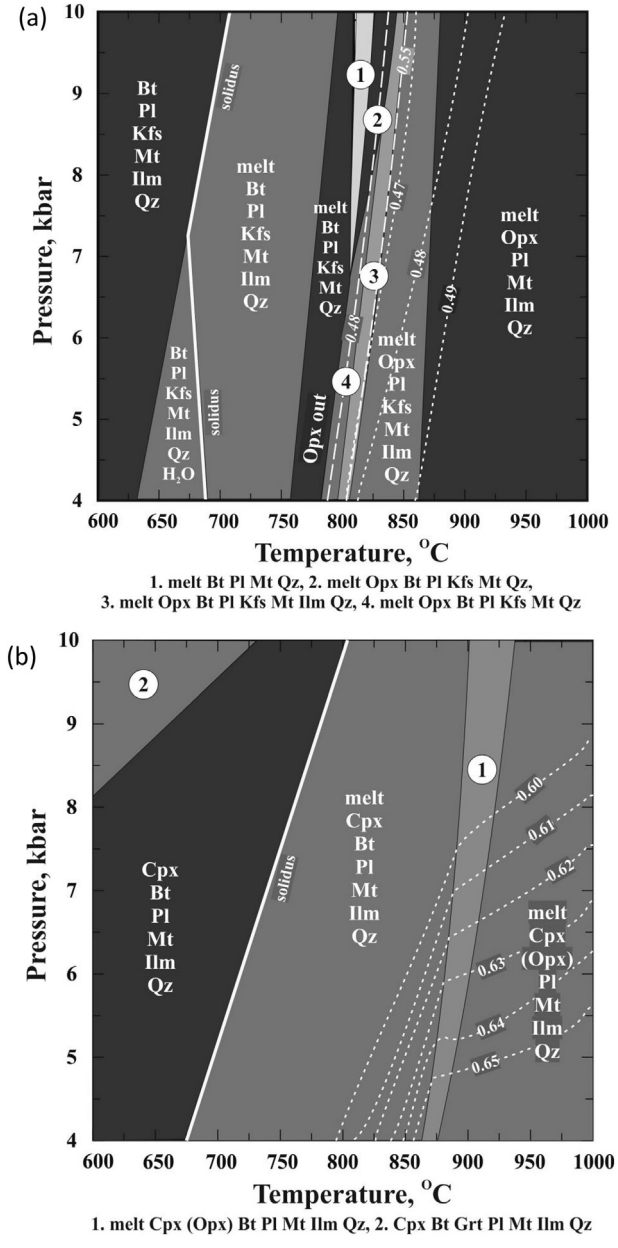

Fig. 9. (a) Pseudosection for the orthopyroxene-bearing granitoid KCH5. (b) Pseudosection for the clinopyroxene-rich granitoid GAB60f.

7.4.1. Orthopyroxene-bearing tonalite-trondhjemites

The orthopyroxene-bearing tonalite-trondhjemites show typical geochemical characteristics of Archean TTG including high Na_2O, Al_2O_3, low K_2O/Na_2O and K-poor calc-alkaline differentiation trend (Fig. 10a). The K-poor, high-Na-Al, calcic composition of these rocks is generally attributed to the derivation from a metabasalt source (Halla et al., 2009; Hoffmann et al., 2011; Martin et al., 2014; Moyen, 2011; Moyen and Martin, 2012; Nagel et al., 2012; Smithies et al., 2009; Zhang et al., 2013). The metabasalt source composition is supported by comparison with melts produced in experiments (Fig. 10b, c). In terms of the chondrite-normalized REE pattern, the orthopyroxene-bearing tonalite-trondhjemites are similar to low-HREE TTG of Halla et al. (2009) (Fig. 8b). Recent studies evaluated the nature of basaltic source that can result in the typical fractionated pattern of low-HREE TTGs [MORB vs enriched MORB (Moyen, 2011); N-MORB vs Isua tholeiite (Nagel et al., 2012); N-MORB vs *E*-MORB (Zhang et al., 2013); MORB-like vs Archean basalt (Martin et al., 2014); see Fig. 10d for a comparison of the common basaltic sources]. Comparison with primitive mantle-normalized trace element patterns of modelled melt compositions from these studies indicate that the orthopyroxene-bearing tonalite-trondhjemites are likely derived from an enriched-MORB-like source (Fig. 11a–c). This supports the general assertion that low-HREE TTGs are formed from a basaltic source that is slightly richer in LILE and LREE than typical MORB (Halla et al., 2009; Hoffmann et al., 2011; Martin et al., 2014; Moyen, 2011; Moyen and Stevens, 2006; Nagel et al., 2012; Smithies et al., 2009; Zhang et al., 2013), consistent with the geochemistry of observed Archean basalts (e.g., Albarède, 2005). Their whole-rock geochemical characteristics, including pressure dependent elements and ratios like Sr/Y, La/Yb, Nb, Ta and Zr/Nb (Bédard, 2006; Halla et al., 2009; Hoffmann et al., 2011; Nagel et al., 2012), show that the orthopyroxene-bearing tonalite-trondhjemites are comparable to the medium-pressure TTGs and different from the high-pressure TTGs (Moyen, 2011) (Fig. 7). Comparison with modelled trends from Moyen (2011) does not discount the possibility of later low-pressure fractionation of the orthopyroxene-bearing tonalite-trondhjemites (see arrowed lines in Fig. 10d).

7.4.2. The significance of clinopyroxene-rich tonalites

In comparison to the orthopyroxene-bearing low-HREE TTGs, the chondrite-normalized REE pattern of the clinopyroxene-rich tonalite is less fractionated and have higher HREE, similar to that of high-HREE TTG of Halla et al. (2009) (Fig. 8b). The clinopyroxene-rich tonalite are enriched in mantle compatible elements (V, Co, Ni) and show higher Mg# than the orthopyroxene-bearing tonalite-trondhjemites. In the Th/Yb versus Nb/Yb diagram of Pearce (2008), the orthopyroxene-bearing tonalite-trondhjemites fall towards the average Archean crustal composition of Rudnick and Fountain (1995), while the clinopyroxene-rich tonalite fall within the MORB-OIB array, close to the E-MORB composition (Fig. 10e). The low silica (~58–59 wt%) clinopyroxene-rich tonalite has unique geochemical characteristics [Mg# = ~42–43, MgO = ~2.7 wt%; V = 95–96 ppm; $(Gd/Er)_N$ = ~1.8–1.9]. Some geochemical characteristics of these rocks are comparable to those of Archean sanukitoids [SiO_2 = 55–70 wt%, Mg# = 45–65, MgO = 1.5–9.0 wt%; V > 50 ppm; $(Gd/Er)_N$ = 2–6; Heilimo et al., 2010]. However, the low-silica rock does not strictly follow the characteristics of the Archean sanukitoids. It has lower K_2O (0.95 wt%), Ba+Sr (583–613 ppm), Cr (~96–103 ppm) and Ni (21–23 ppm) contents (Archean sanukitoids usually show K_2O = 1.5–5 wt%; Ba+Sr > 1400 ppm; Cr > 100 ppm; Ni

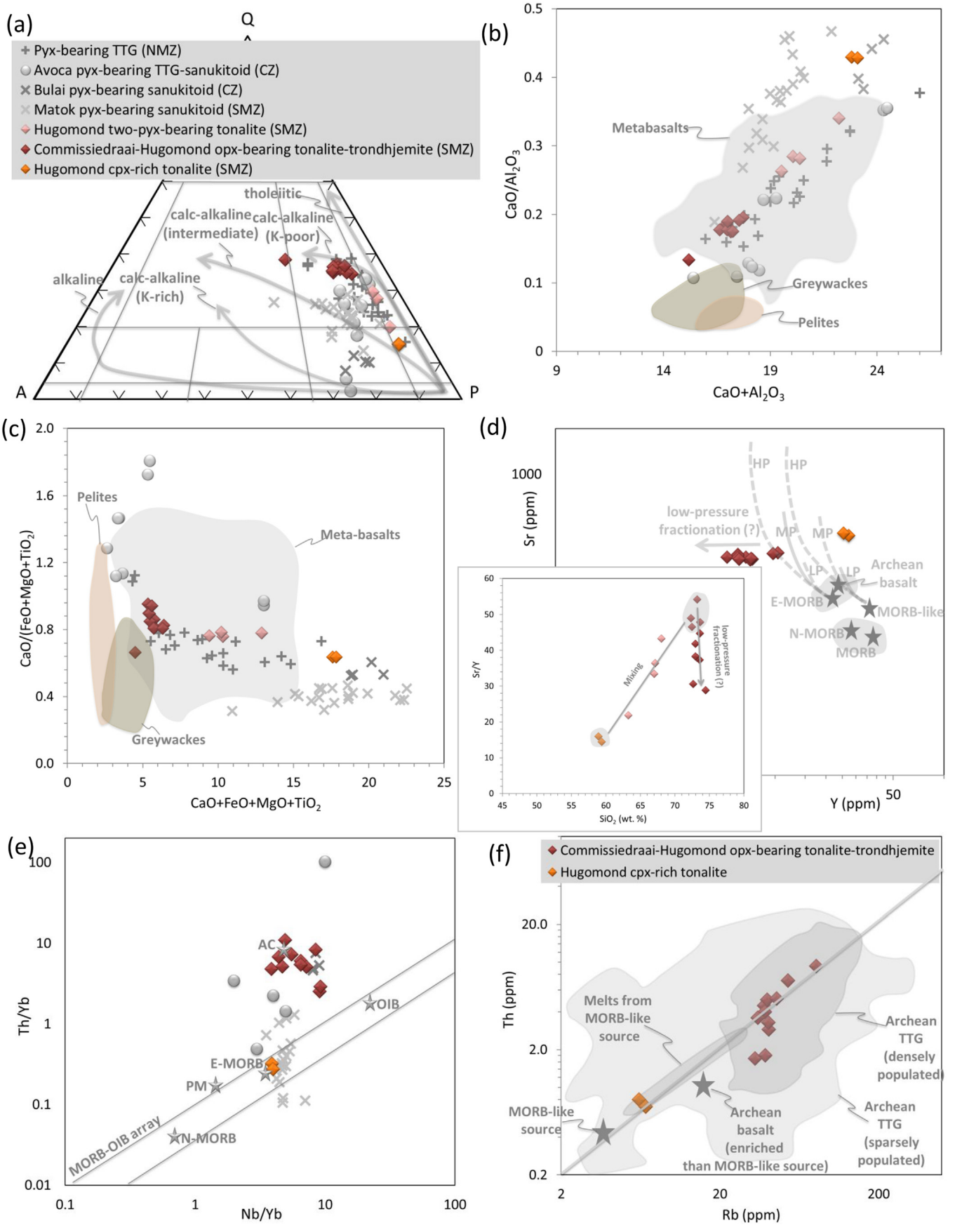

Please cite this article as: H.M. Rajesh, G.A. Belyanin, O.G. Safonov, et al., Pyroxene-bearing low- and high-HREE TTGs from the northeastern margin of the Kaapvaal Craton, southe..., Lithos, https://doi.org/10.1016/j.lithos.2019.105181

> 100 ppm; Heilimo et al., 2010). In this context, it is relevant to compare the compositional characteristics of the studied rocks with other known pyroxene-bearing TTGs and sanukitoids from the Limpopo Complex, such as the pyroxene-bearing TTGs from the Northern Marginal Zone (Berger et al., 1995), the Bulai sanukitoid and Avoca TTG-sanukitoid from the Beit Bridge Complex terrane of the Central Zone (Laurent et al., 2011; Rajesh et al., 2018), and the Matok pyroxene-bearing granitoid with sanukitoid-like composition from the Southern Marginal Zone (Laurent et al., 2014b). The closest correlatives of the Hugomond clinopyroxene-rich tonalite are the Matok and Avoca sanukitoids (Figs. 6 and 7). In spite of the similarities, other features argue against the direct application of the petrogenetic models suggested for these rocks. These include the lack of evidence for the involvement of both crustal and mantle melts, as suggested for the formation of Archean sanukitoids (Halla et al., 2009; Heilimo et al., 2010; Martin et al., 2010), and difference in other geochemical characteristics (Figs. 6, 7 and 10a). Thus, in spite of its TTG-like compositional characteristics, the clinopyroxene-rich tonalites are a unique rock type; probably requiring derivation from a source, which was unique for the Archean.

The mantle geochemical characteristics and enrichment in LREE of the clinopyroxene-rich tonalite indicate contribution from a shallow mantle source. The shallow melting condition is supported by the low Sr/Y, La/Yb, Nb and Ta of clinopyroxene-rich tonalite, similar to low-pressure TTG group of Moyen (2011), and different from the orthopyroxene-bearing tonalite-trondhjemites, which are closer to medium-pressure TTGs (Fig. 7). Comparison with primitive mantle-normalized trace element patterns of modelled melt compositions (Martin et al., 2014; Moyen, 2011; Nagel et al., 2012; Zhang et al., 2013) does not support an enriched-MORB-like source for the clinopyroxene-rich tonalites (e.g., Fig. 11d, e). Significantly, the composition of clinopyroxene-rich tonalite overlap with the calculated melt compositions from a MORB-like source (Moyen and Stevens, 2006; Martin et al., 2014; Fig. 10f). In Fig. 10f, the clinopyroxene-rich tonalite show coupled behaviour of very incompatible elements such as Rb and Th, which is typical of melts of a MORB-like source (see Martin et al., 2014; Moyen and Stevens, 2006). As shown in Fig. 10d, modelled trend (solid line) from a MORB-like source (Moyen, 2011) better accounts for low-pressure (LP) TTGs like clinopyroxene-rich tonalite. This is different from the modelled trend (solid line in Fig. 10d) from an enriched-MORB-like source (Moyen, 2011) which better explains the composition of medium-pressure (MP) TTGs like orthopyroxene-bearing tonalite-trondhjemites. In comparison to the orthopyroxene-bearing tonalite-trondhjemites, the trend towards relatively higher HREE contents, higher Nb/Ta, lower Al_2O_3 and tonalitic composition of the clinopyroxene-rich rock is closer to modelled low-pressure-group-TTG melt compositions from MORB-like source (Willbold et al., 2009; Moyen, 2011; Martin et al., 2014; Fig. 11d, f).

7.4.3. Two-pyroxene bearing tonalites

The geochemical characteristics indicates different trends for the orthopyroxene-bearing and clinopyroxene-bearing granitoids (e.g., Fig. 7 and inset in 10d). Geochronologic data indicate that the clinopyroxene-rich tonalite formed slightly earlier than the orthopyroxene-bearing tonalite-trondhjemites (Retief et al., 1990; Rajesh et al., submitted). Hence both the groups of pyroxene-bearing granitoids cannot be linked by fractionation and cannot represent parts of the same process that would have operated ~10–40 Ma apart. Field relations from the contact zone, characterized by gradational contact between the rounded darker clinopyroxene-rich inclusions and the light greenish-grey two-pyroxene-bearing host, is likely related to the interaction between the clinopyroxene-rich and orthopyroxene-bearing granitoids. Phase equilibria indicate lack of equilibrium between orthopyroxene and clinopyroxene in the two-pyroxene-bearing rock supporting the interaction hypothesis. According to Roeder and Emslie (1970), the test for two-pyroxene equilibrium is that the Fe—Mg exchange coefficient for orthopyroxene-clinopyroxene should be 1.09 ± 0.14. Average compositions of pyroxenes from the studied rocks gave much lower values, about 0.55–0.56. Application of two-pyroxene and single-pyroxene thermometers (e.g., Brey and Köhler, 1990; Putirka, 2008) gave very different values indicating disequilibrium. Together with their linear mixing trends in geochemical diagrams (e.g., see inset in Fig. 10d), the two pyroxene-bearing tonalites is argued to be the product of mingling-mixing between the clinopyroxene-rich and orthopyroxene-bearing TTG endmembers.

7.4.4. Tectonic setting

Inference on likely tectonic setting need to consider the temporal and spatial association of the less dominant clinopyroxene-rich tonalite and the dominant orthopyroxene-bearing tonalite-trondhjemites, their different source compositions (MORB-like versus enriched-MORB-like) and the different depths of melting. Common geodynamic settings in which melting of basaltic sources can be achieved at various depths to produce granitoid rocks of TTG-affinity include subduction of the oceanic lithosphere and plume-related thickened oceanic plateau/tectonically thickened oceanic crust (Bédard, 2006; Halla et al., 2009; Moyen, 2011; Smithies et al., 2009; Willbold et al., 2009). It is important to keep in mind, that the magmas from subducted oceanic crust migrate through mantle en route to the crust, whereas those from melting of thickened plateau/crust do not interact with the mantle. No evidence for mantle-crust interaction is found in the compositional characteristics of the orthopyroxene-bearing and clinopyroxene-rich granitoids. This includes lack of *contradictory* combination of high incompatible (especially K, Ba, Sr, P, and LREE) and compatible (Mg, Cr, and Ni) element composition that could indicate the role of mantle wedge (Halla et al., 2009; Heilimo et al., 2010; Martin et al., 2010). Taking into account of the high-temperatures associated with the formation of anhydrous mineral assemblages (e.g., Bédard, 2003; Frost et al., 2000), melting at different depths in a plume-related oceanic plateau is the likely geodynamic scenario for the formation of the Commissiedraai-Hugomond pyroxene-bearing granitoids. Such an intraplate setting involving melting of the base of the plateau crust above a rising asthenospheric upwelling can provide the heat source to initiate tonalite melt generation (e.g., Bédard, 2006; Smithies et al., 2009). High-pressure melting of subducted oceanic crust in a hotter ambient mantle could also be suitable for the high-temperatures required to form charnockitic assemblages. However, the studied pyroxene-bearing granitoids are comparable to low- to medium-pressure TTGs (Fig. 7).

Fig. 10. Commissiedraai-Hugomond pyroxene-bearing granitoid compositions in terms of QAP plot (a), CaO/Al_2O_3 vs $CaO + Al_2O_3$ plot (b), $CaO/(FeO + MgO + TiO_2)$ vs $CaO + FeO + MgO + TiO_2$ plot (c), Sr vs Y plot (Sr/Y vs SiO_2 plot – inset) (d), Th/Yb vs Nb/Yb plot (e) and Th vs Rb plot (log-log scale) (f). The fields and different trend lines in (a) are from Lameyre and Bowden (1982). Experimental melt compositions produced from pelites, greywackes and metabasalts reviewed by Patiño Douce (1999) are shown in (b) and (c). Models (dashed lines) of melting of mafic sources at different pressures (LP – low pressure; MP – medium pressure; HP – high pressure) in (d) are from Moyen (2011). The trend lines (dashed lines) from Moyen (2011) are modified for the selected source compositions. The two groups of basaltic source compositions, considered as possible source compositions to Archean TTGs are highlighted by the two grey shaded regions. The effect of low-pressure fractionation on TTG compositions is graphically indicated by the arrowed line and is also from Moyen (2011). Such fractionation can typically account for much of the scatter observed in the trends of individual TTG suites (e.g., Moyen, 2011). The fields and typical compositions of primitive mantle (PM), ocean island basalt (OIB), mid-ocean ridge basalt (MORB, N – normal, E – enriched) and Archean crust (AC) in (e) are from Pearce (2008). The different source compositions and fields shown in (f) are from Martin et al. (2014) and references therein.

Please cite this article as: H.M. Rajesh, G.A. Belyanin, O.G. Safonov, et al., Pyroxene-bearing low- and high-HREE TTGs from the northeastern margin of the Kaapvaal Craton, southe..., Lithos, https://doi.org/10.1016/j.lithos.2019.105181

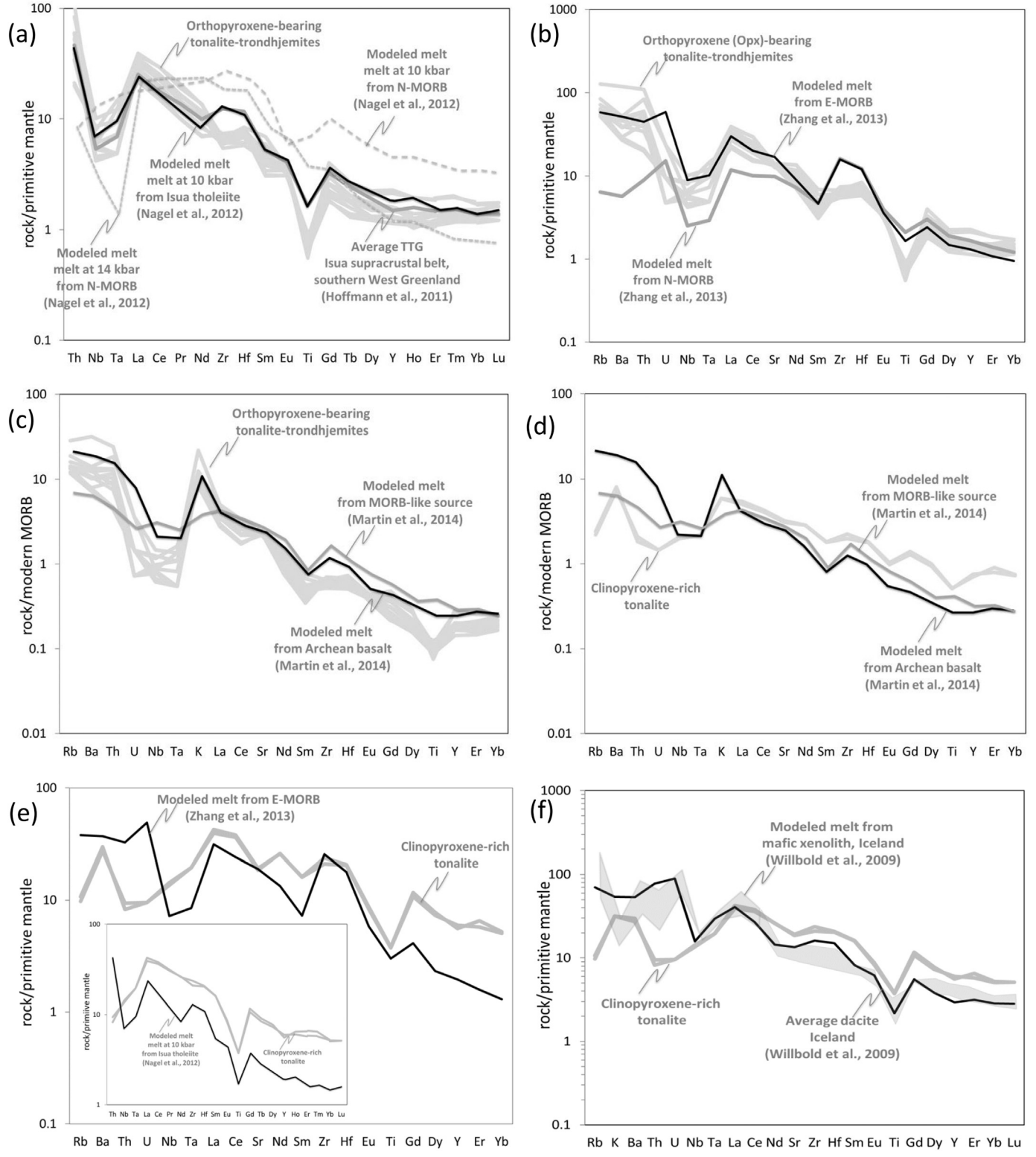

Fig. 11. Primitive mantle-normalized normalized (Sun and McDonough, 1989) (a, b, e, f) and modern MORB normalized (Albarède, 2005; Martin et al., 2014) (c, d) multi-element diagrams comparing Commissiedraai-Hugomond pyroxene-bearing granitoids [orthopyroxene-bearing tonalite-trondhjemites (a to c) and clinopyroxene-rich tonalite (d to f)] with modelled melt compositions from a variety of basaltic source compositions. Modelled N-MORB and Isua tholeiite melt compositions at different pressures (10 and 14 kbars) in (a) and inset in (e) are from Nagel et al. (2012). As shown in (a), average TTG from Isua supracrustal belt, southern West Greenland (from Hoffmann et al., 2011), and having an Archean low-HREE TTG-like composition, is similar to modelled N-MORB melt composition at 10 kbar. Modelled N-MORB and *E*-MORB melt compositions in (b) and (e) are from Zhang et al. (2013). Modelled MORB-like and Archean basalt melt compositions in (c) and (d) are from Martin et al. (2014). Modelled Iceland mafic xenolith melt composition in (f) is from Willbold et al. (2009). As shown in (f), average dacite from Iceland, and having an Archean high-HREE TTG-like composition, is similar to modelled Iceland mafic xenolith melt composition.

Please cite this article as: H.M. Rajesh, G.A. Belyanin, O.G. Safonov, et al., Pyroxene-bearing low- and high-HREE TTGs from the northeastern margin of the Kaapvaal Craton, southe..., Lithos, https://doi.org/10.1016/j.lithos.2019.105181

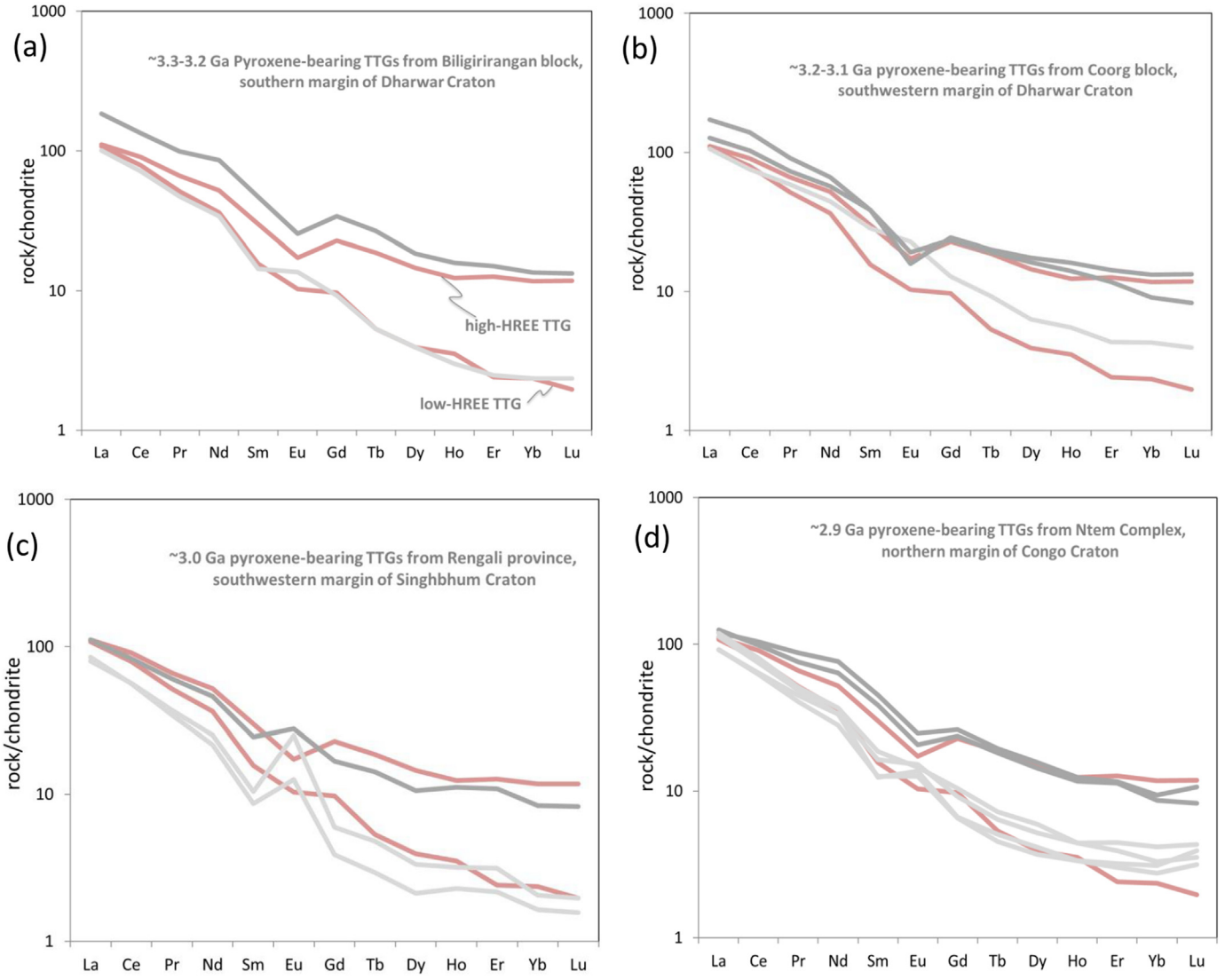

Fig. 12. Chondrite-normalized (Sun and McDonough, 1989) REE plots of well described Mesoarchean pyroxene-bearing TTGs from various high-grade terranes along cratonic margins compared to typical low- and high-HREE TTGs from Halla et al. (2009) (pink lines). (a) ~3.3–3.2 Ga pyroxene-bearing TTGs from the Biligirirangan block, southern margin of Dharwar Craton [data compiled from Mojzsis et al., 2003 and Peucat et al., 2013], (b) ~3.2–3.1 Ga pyroxene-bearing TTGs from the Coorg block, southwestern margin of Dharwar Craton [data compiled from Santosh et al., 2015 and Amaldev et al., 2016], (c) ~3 Ga pyroxene-bearing TTGs from the Rengali province, southwestern margin of Singhbhum Craton [data compiled from Kar et al., 2003] and (d) ~2.9 Ga pyroxene-bearing TTGs from the Ntem Complex, northern margin of Congo Craton [data compiled from Shang et al., 2004 and Pouclet et al., 2007]. (For interpretation of the references to colour in this figure legend, the reader is referred to the web version of this article.)

7.5. Significance of pyroxene-bearing TTGs in Archean geodynamics

7.5.1. What accounts for the presence of pyroxenes in Archean TTGs?

The occurrence of pyroxene is atypical for Archean TTGs. The enriched-MORB-like source suggested for the Mesoarchean Commissiedraai-Hugomond orthopyroxene-bearing tonalite-trondhjemites is comparable to existing models on the origin of TTGs with low-HREE geochemical characteristics. The question then arises on how such an anhydrous mineral be generated in a dry melt that is chemically indistinguishable from the common amphibole- and/or biotite-bearing TTGs. Pyroxenes are peritectic phases during dehydration melting of metabasalts (e.g., Beard and Lofgren, 1991). Orthopyroxene is typical for low- to medium-pressure conditions, while clinopyroxene can crystallize up to high-pressures. Pyroxene-bearing mineral assemblages tend to form readily in Fe-rich granitoids (ferroan in Fig. 6c), whereas Mg-rich bulk compositions tend to rather stabilize biotite and/or amphibole (as it is commonly for TTGs) (Frost et al., 2001). However, the studied pyroxene-bearing TTGs from the Commissiedraai-Hugomond areas are all magnesian (see Fig. 6c). Thus, the presence of pyroxenes in these rocks is not a reflection of their bulk-rock chemistry. Phase equilibria modelling indicate high temperatures and low water activity for the formation of the pyroxene-bearing assemblages in the studied granitoids (Fig. 9). In terms of oxygen fugacity, the prominent association of magnetite with pyroxenes as part of the primary magmatic assemblage (Fig. 4), as also supported by phase equilibria modelling, argues for oxidized conditions to have prevailed during the formation of the pyroxene-bearing granitoids. Thus, it is likely that intrinsic parameters including high temperatures, low water activity and oxidized conditions accounts for the presence or absence of pyroxenes in Archean TTGs.

7.5.2. Pyroxene-bearing high-HREE TTGs as possible MORB-like source derivatives

Unlike the orthopyroxene-bearing tonalite-trondhjemites, the inferred source composition for the Mesoarchean Hugomond clinopyroxene-rich tonalite with high-HREE TTG characteristics is at

odds with geochemical modelling and experimental studies which suggest that a MORB-like source cannot generate TTG magmas (see Martin et al., 2014; Moyen, 2011; Moyen and Stevens, 2006). Reports on Archean MORB-like rocks are scarce. An example is the Mesoarchean MOR-like basaltic rocks from the Clearville area of the West Pilbara Superterrane (Ohta et al., 1996). The MORB-like source composition considered in the present study is slightly enriched than typical MORB and N-MORB, while it is less enriched compared to *E*-MORB and Archean basalt (see the two highlighted fields in Fig. 10d; e.g., Albarède, 2005). Figs. 10d and 11e suggest that an enriched-MORB-like source likely is not able to reproduce the compositional characteristics of the clinopyroxene-rich high-HREE TTG. Modelled melt compositions from a MORB-like source is closer to account for K-poor TTGs like the clinopyroxene-rich rock (see Figs. 10d, f, 11d and f). If our model involving a MORB-like source for clinopyroxene-rich high-HREE TTGs holds ground, then the question arises on whether the occurrence of similar rocks is an indication of MORB-like rocks in the Archean?

7.5.3. Pyroxene-bearing low- and high-HREE TTGs as indicative of oceanic plateau setting

Pyroxene-bearing granitoids (charnockites) manifest two episodes in Archean terranes: Mesoarchean and Neoarchean. The earlier episode (~3.3–2.9 Ga) of pyroxene-bearing granitoid magmatism is restricted to few Archean high-grade terranes along cratonic margins. The ~2.7–2.5 Ga episode is predominant in the Archean, with pyroxene-bearing granitoids covering large tracts along Archean craton margins. The further discussion of the suggested model is restricted to pyroxene-bearing TTGs belonging to the Mesoarchean episode. Well described Mesoarchean pyroxene-bearing TTGs include the ~3.3–3.1 Ga granitoids from the Biligirirangan and Coorg blocks along southern and southwestern margin of Dharwar Craton (Rajesh and Santosh, 2004; Amaldev et al., 2016; Mojzsis et al., 2003; Peucat et al., 2013; Santosh et al., 2015), ~3.1–3.0 Ga granitoids from the Southern Marginal Zone, northeastern margin of Kaapvaal Craton (this study; Rajesh et al., submitted), ~3 Ga granitoids from the Rengali province along the southwestern margin of Singhbhum Craton (Kar et al., 2003) and ~2.9 Ga granitoids from the Ntem Complex at the northern margin of Congo Craton (Pouclet et al., 2007; Shang et al., 2004). These different granitoids occupy minor tracts in the respective high-grade terranes. The pyroxene-bearing rocks in the respective units are dominantly tonalite-trondhjemites. Available geochemical data on the Mesoarchean pyroxene-bearing tonalite-trondhjemites from different Archean high-grade terranes indicate the spatial association of both low-HREE and high-HREE TTGs (Fig. 12). A model involving melting at different depths in an oceanic plateau setting can account for both the temporal and spatial association of pyroxene-bearing low- and high-HREE TTGs. In view of their occurrence in Archean high-grade terranes, an important aspect to keep in mind in the petrogenetic exercise is to properly address the overprint event(s) and their effect on the chemistry of the rocks. Further, low-pressure fractionation is often suggested to account for the dispersal of samples from expected/predicted trends from modelling (e.g., Moyen, 2011) and need to be accounted for.

8. Concluding remarks

Pyroxene-bearing granitoids in high-grade terranes along cratonic margins provide a window into the nature of the Archean lower crust. The present study is an illustration of the wide compositional range of pyroxene-bearing TTGs from Archean high-grade terranes. The pyroxene-bearing Baviaanskloof TTGs in the northeastern margin of the Kaapvaal Craton includes clinopyroxene-rich and orthopyroxene-bearing varieties. Pyroxenes in the studied rocks are magmatic in origin. The lack of textures indicative of pyroxene formation after earlier Fe—Mg minerals, and the paucity of garnet, argue against a metamorphic origin for the pyroxenes. The clinopyroxene-rich tonalites with geochemical characteristics of high-HREE TTGs are similar to low-pressure melts produced in a MORB-like source. The orthopyroxene-bearing tonalite-trondhjemites with geochemical characteristics of low-HREE TTGs are similar to medium-pressure melts from an enriched-MORB-like source. The spatially associated clinopyroxene-rich and orthopyroxene-bearing granitoids are compositionally connected by a two-pyroxene-bearing tonalite as the result of mingling-mixing of the two end members.

Following to their temporal and spatial association, different depths of melting in an oceanic-plateau setting is argued for the formation of the pyroxene-bearing granitoids. First the MORB-like source, above the head of a asthenospheric upwelling, melted at shallow depths to form the high-HREE TTG. Subsequent movement away from the upwelling head towards its tail, resulted in the enrichment of the MORB-like source. Melting of this enriched source occurred at relatively higher depths forming the low-HREE TTG. Such an intraplate setting can certainly account for the high-temperatures, low water activity and possible oxidized conditions that prevailed during the formation of the pyroxene-bearing TTGs.

Supplementary data to this article can be found online at https://doi.org/10.1016/j.lithos.2019.105181.

Acknowledgements

University of Johannesburg and Botswana International University of Science and Technology (BIUST) are thanked for facilities. DDvR acknowledges NRF grant 81040. This study was partially supported by the Russian Scientific Foundation (project no. 18-17-00206 to OGS). Oscar Laurent provided detailed and insightful comments on an earlier version of the manuscript. Comments provided by journal reviewers Jaana Halla and Esa Heilimo helped to further clarify various aspects and produce the present version of the study. Xian-Hua Li is thanked for efficient editorial handling.

References

Albarède, F., 2005. The survival of mantle geochemical heterogeneities. In: Van der Hilst, R.D., Bass, J.D., Matas, J., Trampert, J. (Eds.), Earth's Deep Mantle: Structure, Composition, and Evolution. American Geophysical Union, Washington, DC, pp. 27–46.

Amaldev, T., Santosh, M., Li, T., Baiju, K.R., Tsunogae, T., Satyanarayanan, M., 2016. Mesoarchean convergent margin processes and crustal evolution: petrologic, geochemical and zircon U–Pb and Lu–Hf data from the Mercara Suture Zone, southern India. Gondwana Res. 37, 182–204.

Andersen, D.J., Lindsley, D.H., 1988. Internally consistent solution models for Fe-Mg-Mn-Ti oxides; Fe-Ti oxides. Am. Mineral. 73 (7–8), 714–726.

Barker, F., 1979. Trondhjemite: a definition, environment and hypotheses of origin. In: Barker, F. (Ed.), Trondhjemites, Dacites and Related Rocks. Elsevier, Amsterdam, pp. 1–12.

Barton Jr., J.M., Van Reenen, D.D., 1992. The significance of Rb-Sr ages of biotite and phlogopite for the thermal history of the Central and Southern Marginal Zones of the Limpopo Belt of southern Africa and the adjacent portions of the Kaapvaal Craton. Precambrian Res. 55, 17–31.

Beard, J.S., Lofgren, G.E., 1991. Dehydration melting and water-saturated melting of basaltic and andesitic greenstones and amphibolites at 1, 3 and 6.9 kb. J. Petrol. 32, 465–501.

Bédard, J.H., 2003. Evidence for regional-scale, pluton-driven, high-grade metamorphism in the Archaean Minto Block, northern Superior Province, Canada. J. Geol. 111 183 e 205.

Bédard, J.H., 2006. A catalytic delamination-driven model for coupled genesis of Archaean crust and sub-continental lithospheric mantle. Geochim. Cosmochim. Acta 70 1188 e 1214.

Belyanin, G.A., Kramers, J.D., Vorster, C., Knoper, M.D., 2014. The timing of successive fluid events in the Southern Marginal Zone of the Limpopo Complex, South Africa: constraints from ^{40}Ar- ^{39}Ar geochronology. Precambrian Res. 254, 169–193.

Berger, M., Kramers, J.D., Nägler, T.F., 1995. Geochemistry and geochronology of charnoenderbites in the northern marginal zone of the Limpopo Belt, Southern Africa, and genetic models. Schweizerische Mineralogische und Petrographische Mitteilungen 75, 17–42.

Blenkinsop, T.G., 2011. Archaean magmatic granulites, diapirism, and Proterozoic reworking in the Northern Marginal Zone. Geol. Soc. Am. Mem. 207, 245–268.

Bohlender, F., Van Reenen, D.D., Barton Jr., J.M., 1992. Evidence for metamorphic and igneous charnockites in the Southern Marginal Zone of the Limpopo Belt. Precambrian Res. 55 (1–4), 429–449.

Brey, G.P., Köhler, T., 1990. Geothermobarometry in four-phase lherzolites II. New thermobarometers, and practical assessment of existing thermobarometers. J. Petrol. 31, 1353–1378.

Connolly, J.A.D., 2005. Computation of phase equilibria by linear programming: a tool for geodynamic modeling and its application to subduction zone decarbonation. Earth Planet. Sci. Lett. 236, 524–541.

Du Toit, R., 1994. High Temperature Metasomatic Alteration Associated with Deep Crustal Shear Zones in the Limpopo Belt. Unpublished MSc thesis. Rand Afrikaans University, South Africa 304p.

Du Toit, M.C., Van Reenen, D.D., Roering, C., 1983. Some aspects of the geology, structure and metamorphism of the Southern Marginal Zone of the Limpopo Metamorphic complex. Spec. Publ. Geol. Soc. S. Afr. 8, 89–102.

Frost, B.R., Frost, C.D., Hulsebosch, T.P., Swapp, S.M., 2000. Origin of the charnockites of the Louis Lake Batholith, Wind River Range, Wyoming. J. Petrol. 41, 1759–1776.

Frost, B.R., Arculus, R.J., Barnes, C.G., Collins, W.J., Ellis, D.J., Frost, C.D., 2001. A geochemical classification of granitic rocks. J. Petrol. 42, 2033–2048.

Fuhrman, M.L., Lindsley, D.H., 1988. Ternary-feldspar modeling and thermometry. Am. Mineral. 73 (3–4), 201–215.

Graupner, T., Klemd, R., Henjes-Kunst, F., Goldmann, S., Behnsen, H., Gerdes, A., Dohrmann, R., Barton Jr., J.M., Opperman, R., 2018. Formation conditions and REY enrichment of the 2060 Ma phosphorus mineralization at Schiel (South Africa): geochemical and geochronological constraints. Mineral. Deposita 53 (I8), 1117–1142.

Halla, J., 2005. Late Archean high-Mg granitoids (sanukitoids) in the southern Karelian domain, eastern Finland: Pb and Nd isotopic constraints on crustmantle interactions. Lithos 79, 161–178.

Halla, J., van Hunen, J., Heilimo, E., Hölttä, P., 2009. Geochemical and numerical constraints on Neoarchaean plate tectonics. Precambrian Res. 174, 155–162.

Halla, J., Whitehouse, M.J., Ahmad, T., Bagai, Z., 2017. Archaean granitoids: an overview and significance from a tectonic perspective. Geol. Soc. Lond. Spec. Publ. 449, 1–18.

Harley, S.L., 2004. Extending our understanding of ultrahigh temperature crustal metamorphism. J. Mineral. Petrol. Sci. 99, 140–158.

Heilimo, E., Halla, J., Hölttä, P., 2010. Discrimination and origin of the sanukitoid series: geochemical constraints from the Neoarchean western Karelian Province (Finland). Lithos 115, 27–39.

Hoffmann, J.E., Münker, C., Næraa, T., Rosing, M.T., Herwartz, D., Garbe-Schönberg, D., Svahnberg, H., 2011. Mechanisms of Archean crust formation inferred from high-precision HFSE systematics in TTGs. Geochim. Cosmochim. Acta 75, 4157–4178.

Holland, T., Powell, R., 1996. Thermodynamics of order-disorder in minerals; II, Symmetric formalism applied to solid solutions. Am. Mineral. 81 (11—12), 1425–1437.

Holland, T.J.B., Powell, R., 2011. An improved and extended internally consistent thermodynamic dataset for phases of petrological interest, involving a new equation of state for solids. J. Metamorph. Geol. 29, 333–383.

Kar, R., Bhattacharya, S., Sheraton, J.W., 2003. Hornblende-dehydration melting in mafic rocks and the link between massif-type charnockite and associated granulites, Eastern Ghats Granulite Belt, India. Contrib. Mineral. Petrol. 145, 707–729.

Kreissig, K., Thomas, F.N., Kramers, J.D., Van Reenen, D.D., Smit, C.A., 2000. An isotopic and geochemical study of the northern Kaapvaal Craton and the Southern Marginal Zone of the Limpopo Belt: are they juxtaposed terranes? Lithos 50, 1–25.

Kreissig, K., Holzer, L., Frei, R., Villa, I.M., Kramers, J.D., Kroener, A., Smit, C.A., Van Reenen, D.D., 2001. Geochronology of the Hout River shear zone and the metamorphism in the Southern marginal zone of the Limpopo Belt, Southern Africa. Precambrian Res. 109, 145–173.

Lameyre, J., Bowden, P., 1982. Plutonic rock type series: discrimination of various granitoid series and related rocks. J. Volcanol. Geotherm. Res. 14, 169–186.

Laurent, O., Martin, H., Doucelance, R., Moyen, J.-F., Paquette, J.-L., 2011. Geochemistry and petrogenesis of high-K "sanukitoids" from the Bulai pluton, Central Limpopo Belt, South Africa: implications for geodynamic changes at the Archaean–Proterozoic boundary. Lithos 123, 73–91.

Laurent, O., Martin, H., Moyen, J.F., Doucelance, R., 2014a. The diversity and evolution of late-Archean granitoids: evidence for the onset of "modern-style" plate tectonics between 3.0 and 2.5 Ga. Lithos 205, 208–235.

Laurent, O., Rapopo, M., Stevens, G., Moyen, J.F., Martin, H., Doucelance, R., Bosq, C., 2014b. Contrasting petrogenesis of Mg–K and Fe–K granitoids and implications for post-collisional magmatism: a case study from the late-Archean Matok pluton (Pietersburg block, South Africa). Lithos 196–197, 131–149.

Martin, H., Moyen, J.-F., Rapp, R., 2010. The sanukitoid series: magmatism at the Archaean-Proterozoic transition. Earth Environ. Sci. Trans. R. Soc. Edinb. 100, 15–33.

Martin, H., Moyen, J.-F., Guitreau, M., Blichert-Toft, J., Le Pennec, J.-L., 2014. Why Archaean TTG cannot be generated by MORB melting in subduction zones. Lithos 198–199, 1–13.

Mojzsis, S.J., Devaraju, T.C., Newton, R.C., 2003. Ion microprobe U-Pb age determinations on zircon from the late Archean granulite facies transition zone of southern India. J. Geol. 111, 407–425.

Morimoto, N., Fabries, J., Fergusson, A.K., Ginzburg, I.V., Ross, M., Seifert, F.A., Zussman, J., Aoki, K., Gottard, G., 1988. Nomenclature of pyroxenes. Am. Mineral. 73, 1123–1133.

Moyen, J.F., 2011. The composite Archaean grey gneisses: petrological significance, and evidence for a non-unique tectonic setting for Archaean crustal growth. Lithos 123, 21–36.

Moyen, J.-F., Martin, H., 2012. Forty years of TTG research. Lithos 148, 312–336.

Moyen, J.F., Stevens, G., 2006. Experimental constraints on TTG petrogenesis: implications for Archean geodynamics. In: Benn, K., Mareschal, J.-C., Condie, K.C. (Eds.), Archean Geodynamics and Environments. AGU, pp. 149–178.

Nagel, T.J., Hoffmann, J.E., Münker, C., 2012. Generation of Eoarchean tonalite–trondhjemite–granodiorites series from thickened mafic arc crust. Geology 40, 375–378.

Nicoli, G., Stevens, G., Moyen, J.F., Frei, D., 2015. Rapid evolution from sediment to anatectic granulite in an Archean continental collision zone: the example of the Bandelierkop Formation metapelites, South Marginal Zone, Limpopo Belt, South Africa. J. Metamorph. Geol. 33 (2), 177–202.

Ohta, H., Maruyama, S., Takahashi, E., Watanabe, Y., Kato, Y., 1996. Field occurrence, geochemistry and petrogenesis of the Archaean mid-oceanic ridge basalts(A-MORBs) of the Cleaverville area, Pilbara craton, Western Australia. Lithos 37, 199–221.

Passeraub, M., Wuest, T., Kreissig, K., Smit, C.A., Kramers, J.D., 1999. Structure, metamorphism, and geochronology of the Rhenosterkoppies greenstone belt, South Africa. S. Afr. J. Geol. 102, 323–334.

Patiño Douce, A.E., 1999. What do experiments tell us about the relative contributions of crust and mantle to the origin of granitic magmas? In: Castro, A., Fernandez, C., Vigneresse, J.L. (Eds.), Understanding Granites. Integrating New and Classical Techniques. 158, pp. 55–75 Journal of the Geological Society, Special Publication

Pearce, J.A., 2008. Geochemical fingerprinting of oceanic basalts with applications to ophiolite classification and the search for Archean oceanic crust. Lithos 100, 14–48.

Pearce, J.A., Harris, N.B.W., Tindle, A.G., 1984. Trace element discrimination diagrams for the tectonic interpretation of granitic rocks. J. Petrol. 25, 956–983.

Percival, J.A., 1994. Archaean high-grade metamorphism. In: Condie, K.C. (Ed.), Archaean Crustal Evolution. Elsevier, Amsterdam, pp. 357–410.

Peucat, J.J., Jayananda, M., Chardon, D., Capdevila, R., Fanning, C.M., Paquette, J.-L., 2013. The lower crust of the Dharwar Craton, South India: patchwork of Archean granulitic domains. Precambrian Res. 227, 4–28.

Pouclet, A., Tchameni, R., Mezger, K., Vidal, M., Nsifa, E., Shang, C., Penaye, J., 2007. Archaean crustal accretion at the northern border of the Congo Craton (South Cameroon). The charnockite-TTG link. Bull. Soc. Geol. Fr. 178 (5), 331–342.

Putirka, K.D., 2008. Thermometers and barometers for volcanic systems. In: Putirka, K.D., Tepley III, F.J. (Eds.), Minerals, Inclusions and Volcanic Processes. Mineralogical Society of America and Geochemical Society Reviews in Mineralogy and Geochemistry 69, pp. 61–120 Washington.

Rajesh, H.M., Santosh, M., 2004. Charnockitic magmatism in South India. J. Earth Sys. Sci. 113, 565–585.

Rajesh, H.M., Santosh, M., Yoshikura, S., 2011. The Nagercoil charnockite: a magnesian, calcic to calc-alkalic granitoid dehydrated during a granulite-facies metamorphic event. J. Petrol. 52, 375–400.

Rajesh, H.M., Santosh, M., Wan, Y., Liu, S.J., Belyanin, G.A., 2014. Ultrahigh temperature granulites and magnesium charnockites: evidence for Neoarchean accretion along the northern margin of the Kaapvaal Craton. Precambrian Res. 246, 150–159.

Rajesh, H.M., Belyanin, G.A., Van Reenen, D.D., 2018. Three tier transition of Neoarchean TTG-sanukitoid magmatism in the Beit Bridge Complex, Southern Africa. Lithos 296–299, 431–451.

Retief, E.A., Compston, W., Armstrong, R.A., Williams, L.S., 1990. Characteristics and Preliminary U-Pb Ages of Zircon from Limpopo Belt Lithologies. Abstract volume, Limpopo Workshop, 1990. pp. 95–99.

Ridley, J.R., 1992. On the origins and tectonic significance of the charnockite suite of the Archaean Limpopo Belt, Northern Marginal Zone, Zimbabwe. Precambrian Res. 55, 407–427.

Roeder, P.L., Emslie, R.F., 1970. Olivine-liquid equilibrium. Contrib. Mineral. Petrol. 29, 275–289.

Rollinson, H.R., 1996. Tonalite-trondhjemite-granodiorite magmatism and the genesis of Lewisian crust during the Archean. In: Brewer, T.S. (Ed.), Precambrian Crustal Evolution in the North Atlantic Region. Geological Society, London, Special Publications vol. 112, pp. 25–42.

Rudnick, R.L., Fountain, D.M., 1995. Nature and composition of the continental crust – a lower crustal perspective. Rev. Geophys. 33, 267–309.

Safonov, O.G., Yapaskurt, V.O., Elburg, M., Van Reenen, D.D., Tatarinova, D.S., Varlamov, D.A., Golunova, M.A., Smit, C.A., 2018. P–T conditions, mechanism and timing of the localized melting of metapelites from the Petronella shear zone and relationships with granite intrusions in the Southern Marginal Zone of the Limpopo belt, South Africa. J. Petrol. 59, 695–734.

Santosh, M., Yang, Q.Y., Shaji, E., Tsunogae, T., Mohan, M.R., Satyanarayanan, M., 2015. An exotic Mesoarchean microcontinent: the Coorg Block, southern India. Gondwana Res. 27, 165–195.

Shang, C.K., Satir, M., Siebel, W., Nsifa, N.E., Taubald, H., Liégeois, J.-P., Tchoua, F.M., 2004. TTG magmatism in the Congo craton; a view from major and trace element geochemistry, Rb-Sr and Sm-Nd systematics: case of the Sangmelima region, Ntem complex, southern Cameroon. J. Afr. Earth Sci. 40, 61–79.

Smit, C.A., Roering, C., Van Reenen, D.D., 1992. The structural framework of the southern margin of the Limpopo Belt, South Africa. Precambrian Res. 55, 51–67.

Smit, C.A., Van Reenen, D.D., Roering, C., Boshoff, R., Perchuk, L.L., 2011. Neoarchean to Paleoproterozoic evolution of the polymetamorphic Central Zone of the Limpopo Complex. Geol. Soc. Am. Mem. 207, 213–244.

Smithies, R.H., Champion, D.C., Van Kranendonk, M.J., 2009. Formation of Paleoarchean continental crust through infracrustal melting of enriched basalt. Earth Planet. Sci. Lett. 281, 298–306.

Sun, S.S., McDonough, W.F., 1989. Chemical and isotopic systemics of ocean basalt: Implications for mantle composition and processes. In: Saunders, A.D., Norry, M.J. (Eds.), Magmatism in the Ocean Basins. Geological Society, London, Special Publications vol. 42, pp. 313–345.

Sylvester, P.J., 1994. Archean granite plutons. In: Condie, K.C. (Ed.), Archean Crustal Evolution. Developments in Precambrian Precambrian Geology vol. 11. Elsevier, Amsterdam, pp. 261–314.

Taylor, J., Nicoli, G., Stevens, G., Frei, D., Moyen, J.F., 2014. The processes that control leucosome compositions in metasedimentary granulites: Perspectives from the Southern Marginal Zone migmatites, Limpopo Belt, South Africa. J. Metamorph. Geol. 32 (7), 713–742.

Tsunogae, T., Van Reenen, D.D., 2014. High- to ultrahigh-temperature metasomatism related to brine infiltration in the Neoarchaean Limpopo Complex. Petrology and phase equilibrium modeling. Precambrian Res. 253, 157–170.

Please cite this article as: H.M. Rajesh, G.A. Belyanin, O.G. Safonov, et al., Pyroxene-bearing low- and high-HREE TTGs from the northeastern margin of the Kaapvaal Craton, southe..., Lithos, https://doi.org/10.1016/j.lithos.2019.105181

Van Reenen, D.D., 1986. Hydration of cordierite and hypersthenes and description of the retrograde orthoamphibole isograd in the Limpopo Belt, South Africa. Am. Mineral. 71, 900–915.

Van Reenen, D.D., Smit, C.A., Perchuk, L.L., Roering, C., Boshoff, R., 2011. Thrust exhumation of the Neoarchean ultrahigh-temperature Southern Marginal Zone, Limpopo Complex: Convergence of dempression-cooling paths in the hanging wall and prograde-P-T paths in the footwall. Geol. Soc. Am. Mem. 207, 189–212.

Vezinet, A., Moyen, J.F., Stevens, G., Gautier, N., Laurent, O., Couzinié, S., Frei, D., 2018. A record of 0.5 Ga of evolution of the continental crust along the northern edge of the Kaapvaal Craton, South Africa: Consequences for the understanding of Archean geodynamic processes. Precambrian Res. 305, 310–326.

White, R.W., Powell, R., Holland, T.J.B., Worley, B.A., 2000. The effect of TiO_2 and Fe_2O_3 on metapelitic assemblages at greenschist and amphibolite facies conditions: mineral equilibria calculations in the system K_2O-FeO-MgO-Al_2O_3-SiO_2-H_2O-TiO_2-Fe_2O_3. J. Metamorph. Geol. 18 (5), 497–511.

White, R.W., Powell, R., Holland, T.J.B., Johnson, T.E., Green, E.C.R., 2014. New mineral activity–composition relations for thermodynamic calculations in metapelitic systems. J. Metamorph. Geol. 32, 261–286.

Willbold, M., Hegner, E., Stracke, A., Rocholl, A., 2009. Continental geochemical signatures in dacites from Iceland and implications for models of early Archaean crust formation. Earth Planet. Sci. Lett. 279, 44–52.

Zeh, A., Gerdes, A., Barton Jr., J.M., 2009. Archean accretion and crustal evolution of the Kalahari Craton – the zircon age and Hf isotope record of granitic rocks from Barberton/Swaziland to the Francistown Arc. J. Petrol. 50, 933–966.

Zhang, C., Holtz, F., Koepke, J., Wolff, P.E., Ma, C., Bédard, J., 2013. Constraints from experimental melting of amphibolite on the depth of formation of garnet-rich restites, and implications for models of Early Archean crustal growth. Precambrian Res. 124, 327–341.

Please cite this article as: H.M. Rajesh, G.A. Belyanin, O.G. Safonov, et al., Pyroxene-bearing low- and high-HREE TTGs from the northeastern margin of the Kaapvaal Craton, southe..., Lithos, https://doi.org/10.1016/j.lithos.2019.105181